# Neurospectroscopy: The Past, Present and Future

Carolyn E. Mountford,*,† Peter Stanwell,† Alexander Lin,†,‡ Saadallah Ramadan,† and Brian Ross‡

*Centre for Clinical Spectroscopy, Department of Radiology, Brigham & Women's Hospital, Harvard Medical School, 4 Blackfan Street, HIM-817, Boston, Massachusetts 02115, Clinical Spectroscopy, Huntington Medical Research Institutes, Pasadena, California 91105*

*Received July 14, 2009*

## Contents



* To whom correspondence should be addressed. E-mail: cmountford@bics.bwh.harvard.edu. Phone: +1 617 750 3310. Fax: +1 617 525-5047.
† Harvard Medical School.
‡ Huntington Medical Research Institutes.

## 1. Introduction

To the chemist, nuclear magnetic resonance (NMR) spectroscopy has become a necessary tool for decoding the molecular structure of compounds. To quote Loudon, "since its introduction in the late 1950s, NMR spectroscopy has revolutionized organic chemistry".[1] This same technique, applied to the human body, has revolutionized biochemistry and now medicine in this new millennium. Utilizing many of the same underlying principles familiar to chemists, physicians and medical physicists have a diagnostic examination that is capable of early detection of disease, monitoring medical therapies or treatments, and in some cases, negating the need for surgical procedures. This valuable new tool is called magnetic resonance spectroscopy (MRS) or to some "the virtual biopsy".

The concept of using NMR to study the human body is by no means new. In fact, as reported by Andrew,[2] Bloch in 1946 obtained a strong proton signal by placing his finger in the radiofrequency coil of his spectrometer. The potential of using NMR to study biological systems was discussed throughout the 1950s and early 1960s; it was not until the advent of high-field superconducting magnets together with

10.1021/cr900250y © 2010 American Chemical Society
Published on Web 04/13/2010

Carolyn E. Mountford is currently the Director of the Centre for Clinical Spectroscopy at the Brigham and Women's Hospital and Harvard Medical School. She earned her D.Phil. degree in biophysics and biochemistry from Somerville College, University of Oxford. Dr. Mountford has authored many peer-reviewed articles, book chapters, and textbooks. She is a Foundation Fellow of the ISMRM. As CEO of the Institute for Magnetic Resonance in Medicine at the University of Sydney, she trained many surgeons, pathologists, and scientists in the application of clinical spectroscopy. She is an inventor on several patents pertaining to the clinical application and interpretation of clinical MR spectroscopy. Dr. Mountford chaired the Australian Science Engineering and Technology Council study for the development of guidelines for the ethics and scientific management of Australian world heritage and protected areas.

Peter Stanwell is a Clinical Physicist, Spectroscopist, and registered MRI Technologist (RT) at the Center for Clinical Spectroscopy, Brigham and Women's Hospital. He is also an Instructor in Radiology at Harvard Medical School. Dr. Stanwell received his initial B.Sc. from The University of Newcastle and a subsequent Graduate Diploma in MRI from Johns Hopkins Medical Institutions. His Ph.D. was awarded by the University of Sydney's Department of Magnetic Resonance in Medicine. In addition to holding a Ph.D., he is an RT with 16 years clinical experience using MRI. He has worked closely with treating physicians to develop MR techniques with direct clinical applicability and has been instrumental in the development and implementation of new MR techniques for applications in the brain, breast, ovary, and thyroid and to diseases including mesothelioma and melanoma. He has been integral to the development of MRS techniques for the investigation of chronic pain.

the emergence of fast Fourier transform (FFT) that the potential become a reality.[3] At that same time, scientists began to realize that NMR equipment could produce images of the body, which led to the advent of magnetic resonance imaging (MRI) as we know it today.[4] This introduced the wide bore horizontal magnets that we know today as MR "scanners".

It is rather ironic that despite its origins in FFT spectroscopy, NMR (now known as magnetic resonance spectroscopy (MRS)) is only now beginning to enter the realm of medicine

Alexander P. Lin, Ph.D., is a MR Spectroscopist at the Center for Clinical Spectroscopy at Brigham and Women's Hospital and Assistant Professor of Radiology at Harvard Medical School. Dr. Lin completed his Masters degree in Bioengineering and his doctoral degree in Biochemistry and Molecular Biophysics at the California Institute of Technology. He was appointed Director of Clinical Services and Senior Scientist at the Magnetic Resonance Spectroscopy Unit at the Huntington Medical Research Institutes in 2003. Since then he was visiting research associate at the Center of MR Research of the University of Illinois, Chicago, and undertook a research fellowship at the National Heart, Lung and Blood Institute at the NIH. Dr. Lin commenced at the Brigham and Women's Hospital in 2009 and his research interests include clinical applications of proton and multinuclear magnetic resonance spectroscopy in the brain, breast, and liver and cardiovascular magnetic resonance imaging. He was awarded the Young Investigator's Award in 2003 for his work in $^{13}C$ spectroscopy in Alzheimer's disease and NHLBI Fellows Research Award for his work in strain mapping of the carotid arteries.

Saadallah Ramadan is a Spectroscopist and Physicist at the Center for Clinical Spectroscopy at Brigham and Women's Hospital and Instructor in Radiology at Harvard Medical School. Dr. Ramadan received his Ph.D. from the University of Sydney. This was followed by a position as a research scientist in the Departments of Biochemistry and Chemistry at the University of Sydney. Dr. Ramadan became a Research Fellow at the Institute for Magnetic Resonance in Medicine at the University of Sydney where he commenced *in vivo* MRS studies and was subsequently awarded a prestigious ARC Discovery Grant to develop two-dimensional MR spectroscopic techniques for human *in vivo* applications. In late 2007, he moved to the Brigham and Women's Hospital in Boston to assist in the establishment of the Center for Clinical Spectroscopy where his 2D technology is now applied *in vivo* effectively to multiple organs and diseases.

two decades behind MRI. The first organ where the MRS method was employed clinically is the brain and the technique became known as "neurospectroscopy". Neurospectroscopy was reported in the late 1980s and early 1990s by Luyten and Denhollander[5−11] when data from healthy and glioblastoma subjects were acquired. Developmental work by Frahm et al. also started at the same period where short

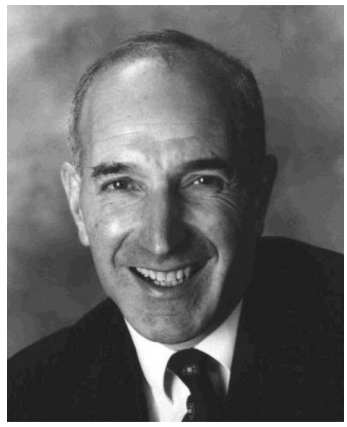

Brian D. Ross is the Director of the Magnetic Resonance Spectroscopy Unit at the Huntington Medical Research Institutes in Pasadena, California. He earned his D.Phil. degree in biochemistry at Trinity College, University of Oxford, and M.D. at University College Hospital in London and University of Southern California. Dr Ross, an accredited surgeon, pathologist, radiologist, and neurologist, has authored numerous publications and teaching chapters. He instituted the first comprehensive clinical MRS service in the United States and is the inventor of the magnetic resonance spectral analysis of the brain for diagnosis of clinical applications. He has also trained hundreds of physicians, scientists, and technologists in the acquisition and interpretation of data in this essential diagnostic technique. He was awarded a Gold Medal by the International Society of Magnetic Resonance in Medicine in 1995 for recognition of his work in this field.

echo time neurospectroscopy exams were implemented and brain metabolites were quantified.[12−17] Then in the mid-1990s the first automated MRS exam, called "proton brain examination (PROBE)", was developed by a major MR manufacturer in conjunction with Dr. Brian Ross.[18] Shortly after, MRS received Food and Drug Administration (FDA) approval and a medical billing Current Procedural Terminology code (CPT 76390), which has brought it from the realm of academic research to that of the hospital clinic.[19] The hardware necessary to undertake MRS is the same as that needed for MRI but with additional software. Now all major MR manufacturers have relatively automated software to facilitate neurospectroscopy.

This review will concentrate on MRS of the human brain (neurospectroscopy) and be restricted to the proton nucleus and its use to diagnose diseases and pain in the clinic. Data from three different magnetic field strengths will be described, 1.5, 3.0, and 7.0 T, illustrating the increase in spectral resolution associated with the increased magnetic field strength, and the technical issues to be faced at 7 T.

There are four basic premises to be considered when using MRS to study cells, tissues, organs, and humans *in vivo*:

1. Those chemicals recorded are in pools that are visible on the MR time scale. Macromolecules such as DNA and RNA are not mobile on the MR time scale but are part of a very broad underlying and unresolved spectrum.
2. Some chemicals can be present in several different spatial locations, each with a different rate of molecular motion and hence relaxation rate. The term quantification is thus often a misnomer because the intensity of the resonance may not be reflective of the total concentration of that chemical in the specimen in question.
3. Many of the recorded chemicals alter with aging, immune response, and development of disease.[20,21] In addition, many of these biochemical processes occur in parallel but do not necessarily alter in the same direction. Thus care in interpretation is needed as is a basic understanding of the biochemistry associated with these spectral alterations.
4. Each voxel in a neurospectroscopy study is likely to contain a mixture of gray and white matter and, if diseased, a heterogeneous population of cell types. Thus as suggested above, absolute quantification of the metabolites is not realistic. Instead resonance ratios or pattern recognition methods are usually implemented. There are approximately 35 metabolites measurable in the human brain by either *in vitro* or *in vivo* MRS methods (Figure 1). The structure of these neurochemicals, proton MR spectra, chemical shifts, and coupling constants, obtained at high field, are reported by Govindaraju and colleagues.[22]

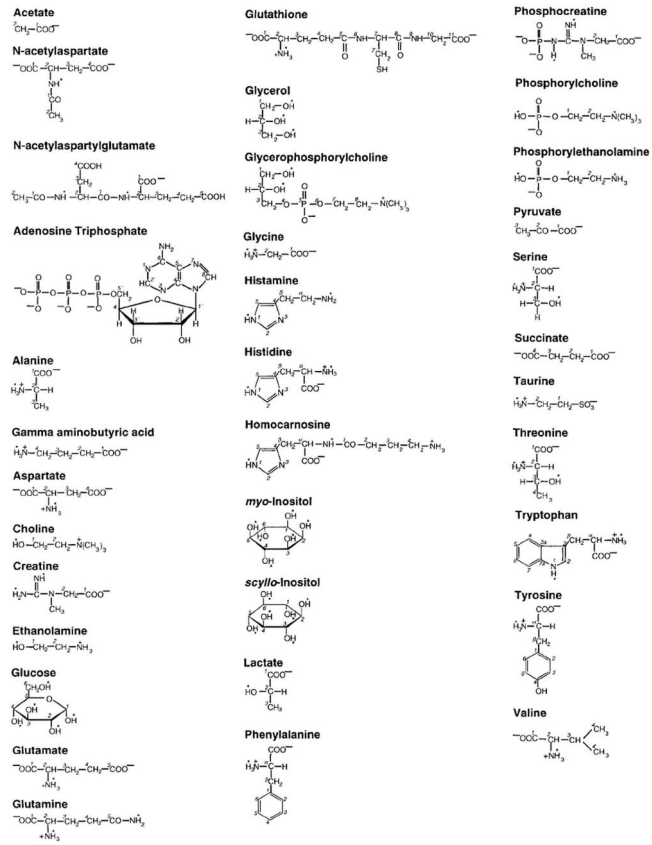


**Figure 1.** Metabolites in the human brain. Chemical structures for metabolites observable by proton MRS in mammalian brain. Exchangeable protons are indicated by the asterisks and assignments of the molecular groups follow the IUPAC nomenclature. Reprinted with permission from Govindarju et al.[22] *NMR Biomed*. Vol. 13, p 132. Copyright 2000 Wiley-Blackwell.

The molecules that are recordable in the healthy brain using neurospectroscopy at 1.5 T are shown in Figure 2. It will be seen, throughout the review, that at the lower field strength of 1.5 T, a small proportion of these molecules are available for inspection due to spectral overlap. However at 3 T and then 7 T many molecules become available for inspection due to increased spectral dispersion and signal-to-noise ratio (SNR). Some chemicals only appear with certain disease states or with altered biochemistry. Some of these are described below.

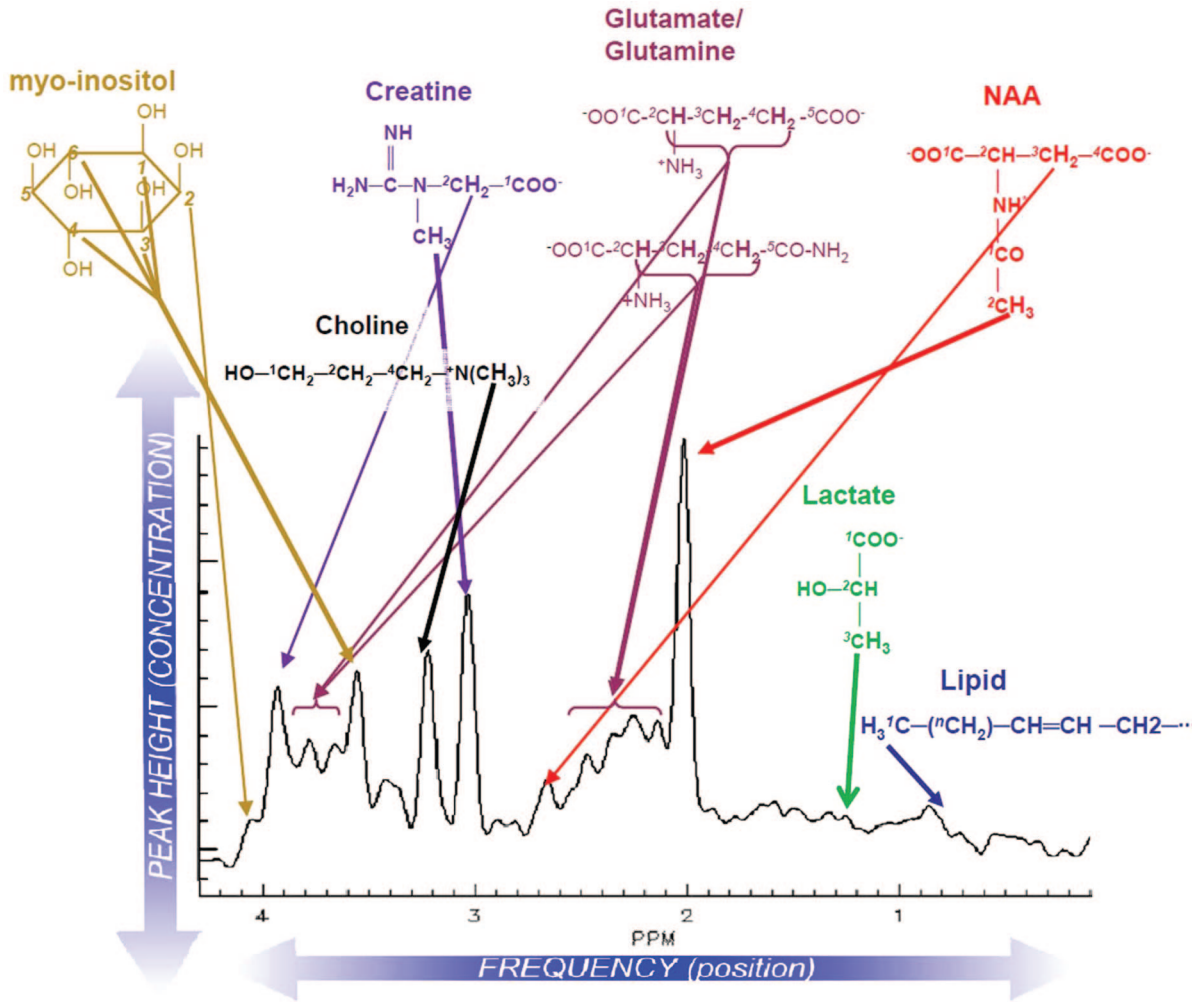


**Figure 2.** MRS from heatlthy human brain at 1.5 T. A typical PRESS spectrum (TE = 35 ms, TR = 1500 ms) from the human brain. Each resonance is labeled with the molecule and its structure. Note that lipid and lactate are not present in healthy brain (as shown here) and therefore their resonances are not visible. Reprinted from *NeuroRX*, Vol. 2, Lin et al, Efficacy of proton magnetic resonance spectroscopy in neurological diagnosis and neurotherapeutic decision making, pp 197−214, 2005 with permission from Elsevier.[46]

## 2. The Present and the Past

### 2.1. The Healthy Brain at 1.5 T

The early work to develop neurospectroscopy was undertaken at 2 T by Frahm and colleagues[23] and at 1.5 T by Dr. Brian Ross and colleagues.[24,25] A typical spectrum obtained from a 29 year old healthy volunteer at 1.5 T is shown in Figure 2, where the key brain metabolites are identified.[24,26,27] Differences between the gray and white matter are recorded at 1.5 T, for example, in the ratio of choline to creatine and creatine to myoinositol (Figure 2), as described in Danielsen and Ross.[24] There are also alterations to the spectral profiles that are age related. The field strength of the magnet causes changes in the resonance ratios due to frequency dependence as is seen later in this review (section 5).

It is helpful to understand the biochemical relevance of each of the major resonances in the brain spectra. These are described as follows.

#### *2.1.1. N-Acetylaspartate (NAA)*

The acetyl moiety of NAA is clearly visible at 2.02 ppm. NAA is an amino-acid derivative synthesized in neurons and transported down axons. It is therefore an almost 100%-specific; immunohistochemical labels show NAA to be distributed throughout the neuron and axon (Figure 3).[28] Several studies have correlated the concentration of NAA in the brain with the number of neurons measured.[28] The ability to relate the NAA resonance to neuron populations allows MRS to provide a diagnostic tool that no other radiological technique can match. For example, if an area of the brain has focal disease, for example, abscess or tumor, then the NAA signal will be significantly reduced and replaced by the chemical signature of that disease process. Nearly all the diagnostic applications of neurospectroscopy involve the measurement of NAA as a diagnostic marker for disease.[29] Due to its importance, a further exploration of this neurochemical marker is given.

#### *2.1.2. Metabolism of NAA and The Peptide N-Acetylaspartylglutamate (NAAG)*

In the metabolism of NAA, the transamination of glutamate with oxaloacetate leads to aspartate[30] (Figure 4). In the presence of acetyl CoA and an NAA synthase (L-asparatate *N*-acetyltransferase), aspartate is converted to *N*-acetylaspartate. This process occurs primarily, but not exclusively, in neurons, where it exhibits a very high intracellular−extracellular gradient. NAA is hydrolyzed back into aspartate and acetate by aspartoacylase (*N*-acetyl-L-aspartate amidohydro-

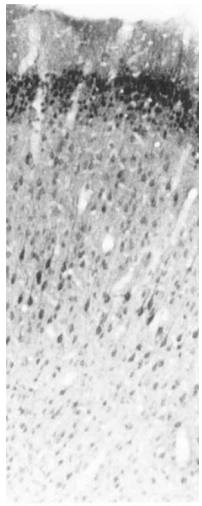

**Figure 3.** NAA Micrograph. NAA-specific stains demonstrate that NAA is localized in neurons and axons. Reproduced,[28] with permission, from Moffet et al. "Enhanced Carbodiimide Fixation for Immunohistochemistry: Application to the Comparative Distributions of N-acetylaspartylglutamate and N-acetylaspartate Immunoreactivities in Rat Brain" *Journal of Histochemistry & Cytochemistry*, Vol 41, pp 559−570, 1993.

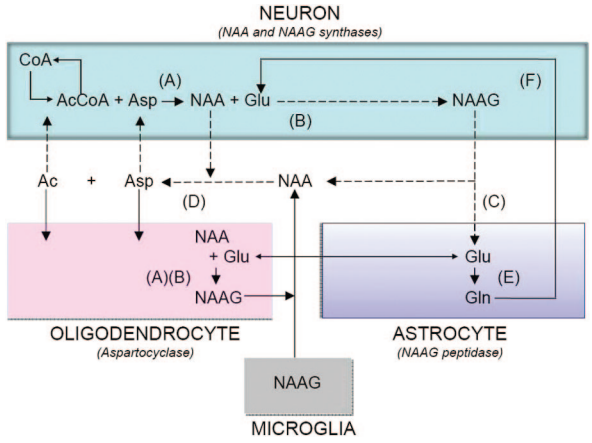


**Figure 4.** NAA−NAAG cycle. Tricellular NAA−NAAG cycle operating between neurons, astrocytes, and oligodendrocytes. Data obtained from B. D. Ross and A. Lin.

lase) in mature oligodendrocytes only. In some neurons, a portion of NAA is turned into NAAG in the presence of glutamate by an NAAG synthase (*N*-acetylaspartate-L-glutamate ligase). On the surface of astrocytes, the catabolic enzyme NAAG peptidase (glutamate carboxypeptidase) cleaves NAAG to NAA and Glu.[31]

### 2.1.3. Functions of the NAA and NAAG Systems

NAA and NAAG are major neuronal osmolytes, and the large amount of NAA and NAAG present in the brain can serve as cellular reservoirs for aspartate and glutamate. Since both are polar and ionizable hydrophilic molecules that undergo a regulated efflux into extracellular fluid, they can also play a role in water movement out of neurons.[31] In addition, the fact that the NAA metabolizing enzyme aspartoacylase is an integral component of the myelin sheath suggests that intraneuronal NAA may supply the acetyl groups for myelin lipid synthesis.[32]

Finally, the cell-type specific metabolic enzymes in the NAA and NAAG cycle indicate a three-cell compartmentalization involving neurons, astrocytes and oligogendrocytes. Those neurons that may synthesize NAAG from NAA and glutamate target the release of NAAG to astrocytes, where it is cleaved into NAA and glutamate. The glutamate is taken up by astrocytes, where it may be returned to neurons via the glutamate−glutamine cycle. The residual NAA extracellular products are removed and hydrolyzed by oligodendrocytes (Figure 4). This unique tricellular metabolic cycle involving NAA and NAAG provides a potential glial cell-specific signaling pathway.[31]

### 2.1.4. Glutamate and Glutamine

Collectively, glutamate and glutamine are sometimes referred to as Glx. The reason for this is that at 1.5 T (but not at 7 T), the spectral resonances overlap. They are a mixture of closely related amino acids involved in brain neurotransmission that lies between 2.12 and 2.35 ppm ($\beta-\gamma$ region) as well as 3.74 and 3.75 ppm (α-region). Glutamine is an astrocyte marker that contributes primarily to the $\beta-\gamma$ region and is often found increased in diseases such as hepatic encephalopathy, Reyes syndrome, hypoxic−ischemic events, and hyperosmolar states and decreased in Alzheimer's disease and hyponatremia.[33] Recent $^{13}C$ MRS experiments in the human brain using both $^{13}C$-labeled glucose and $^{13}C$-labeled acetate have elucidated the glutamate synthesis pathway demonstrating the long-recognized two metabolic pools in astrocytes and neurons. In addition, these $^{13}C$ results have verified the proton MRS results.[34]

### 2.1.5. Creatine

The primary resonance of creatine, $N(CH_3)$, is at 3.02 ppm. This resonance is primarily due to creatine and phosphocreatine, which are in constant rapid enzymatic chemical exchange. Phosphocreatine plays a crucial role in adenosine triphosphate (ATP) synthesis and is therefore used as the central energy marker of both neurons and astrocytes. Generally "constant" in the normal brain spectrum, creatine is often used as an internal standard to scale other metabolites. This can be a dangerous assumption because some systemic (noncerebral) diseases can cause changes to cerebral creatine concentrations. The reason for this effect is that creatine is transported into the brain from the liver as demonstrated by a decrease in cerebral creatine in liver diseases but replenishment after a successful liver transplant (Figure 5).[35]

### 2.1.6. Choline

Choline (Cho) is a misnomer for several soluble components of brain myelin and fluid cell membranes including phosphocholine and glycerolphosphocholine. The main choline resonance, $N(CH_3)_3$, in the brain spectrum resonates at 3.21 ppm. Because by far the majority of choline-containing brain constituents are not normally soluble, pathological alterations in membrane turnover (tumor, leukodystrophy, multiple sclerosis) result in a massive increase in MRS visible products of phosphatydilcholine, phosphoryl choline (PC), and glycerophosphoryl choline, along with their ethanolamine analogues,[35] providing important diagnostic information. Proton-decoupled $^{31}P$ MRS has elucidated some of the neurochemical pathways of the choline/ethanolamine series constituents, which may result in further diagnostic value.[35]

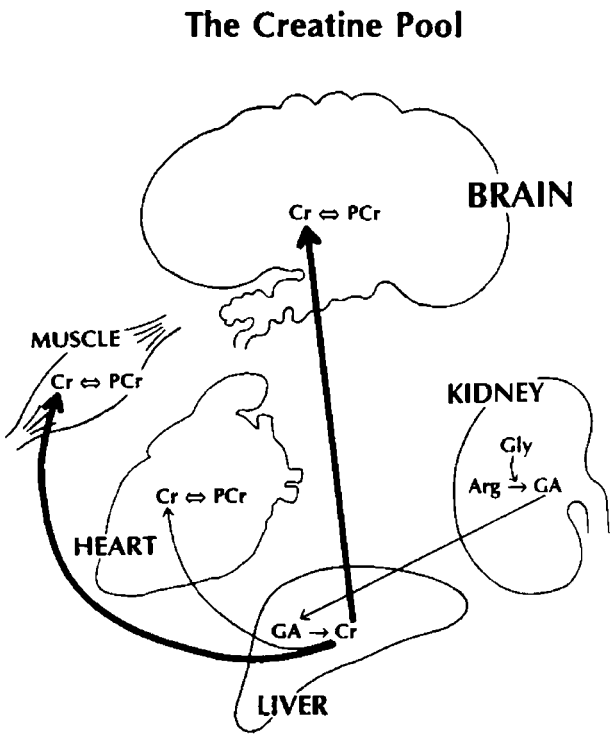


**Figure 5.** Creatine metabolism in different parts of the body and how it relates to cerebral creatine concentrations. Reprinted with permission from ref 154. Copyright 2001 Wiley-Blackwell.

### 2.1.7. Myoinositol

The C4 of myoinositol (mI), a six-carbon polyol, resonates at 3.6 ppm although its enantiomer, scylloinositol resonates at 3.34 ppm. Myoinositol is by itself not usually diagnostic. However when used in combination with other changes in metabolites, it becomes a diagnostic "modifier" in diseases that affect choline (tumor, multiple sclerosis etc). As an astrocyte marker and osmolyte, mI contributes specificity in dementia diagnosis[36] and is almost absolutely specific for hepatic encephalopathy and hyponatremic brain syndromes.[37]

Myoinositol generates four groups of resonances; a doublet-of-doublets centered at 3.52 ppm and a triplet at 3.61 ppm are the two prominent multiplets each corresponding to two protons. A triplet at 3.27 ppm is typically hidden under choline, and another at 4.05 ppm is sometimes not observed because of water suppression.

### 2.1.8. Lipids

Lipids in the brain are composed of a variety of long-chain fatty acids that result in broad resonances at 0.90 ppm ($\mathbf{CH_3}$-$(CH_2)_n$-) and 1.30 ppm (-$(\mathbf{CH_2})_n$-) in a healthy brain spectrum (Figure 2). If the lipids are unsaturated in nature, a resonance will be seen at 5.40 ppm from the −CH=CH−.

Although lipids are present throughout the brain in the form of membranes, few are "MR visible" in healthy tissues. If they are mobile on the MR time frame, it reflects a disease process taking place, for example, tumor or trauma. In healthy tissues, there should be very little lipid in the spectrum unless the area from which the data is acquired lies too close to the skull, in which case the lipid signal arises from subcutaneous tissues, meninges, or the skull itself. Within the brain, the presence of lipid indicates necrosis or hypoxia where severity of injury correlates with the amount of lipid liberated[38] and a variety of hereditary leukodystrophies.

### 2.1.9. Lactate

Lactate is seen in the spectrum as a doublet at 1.33 ppm. Healthy tissues do not have sufficient lactate to be detectable by MRS. However, lactate as a product of anaerobic glycolysis is detected in diseased brain when oxygen-starved. In addition, interruption of the Krebs cycle by mitochondrial damage, absence or inhibition of pyruvate dehydrogenase (the enzyme that generates the two-carbon fragments that are to enter the TCA cycle), and acceleration of glycolysis itself (in tumors and "recovering hypoxic tissue") result in detectable lactate.[39] Detection of lactate due to these pathological processes is of great diagnostic value in cases of brain injury or trauma where hypoxia is part of the differential.[40] It is also a nonspecific marker of tumor aggressiveness and abscesses of all types.

### 2.1.10. Macromolecules

In the same region as lipid and lactate, there are also macromolecules of high molecular weight, such as proteins, that coresonate at 0.93, 1.24, 1.43, 1.72, 2.05, 2.29, and 3.00 ppm, labeled as M1−M7, respectively.[41] While the precise chemical structure of these macromolecules is unclear, they can be identified as broad resonances that underlie 0.9−3.0 ppm in conventional short echo MRS (TE < 30 ms). More importantly, they have different $T_1$ and $T_2$ relaxation times, which allows them to be characterized using selective editing of *J*-coupled resonances, described as metabolite or spectral "nulling". In addition, methods such as 2D correlation spectroscopy (COSY) experiments[42−44] and advanced spectral analysis, as will be described later in this review, would also be capable of characterizing these macromolecules. It is possible that characterizing these resonances will provide additional diagnostic value to proton MRS.

### 2.1.11. Additional Resonances to Consider

Neurospectroscopy provides information on brain constituents not all of which are expected! Recognizable molecules include alcohol; methylsulfonylmethane (MSM),[45] a common health food supplement; mannitol and propylene glycol, common medications; and glucose, acetate, acetone, succinate, and phenylalanine, all defined by their chemical shift (ppm). The unexpected appearance of these molecules adds "spice" and diagnostic specificity to the clinical practice of neurospectroscopy.[34]

Every metabolite has a "normal" ratio that generates a pattern of resonances that is the same from person to person unless there is an underlying pathology. Diagnosis with neurospectroscopy can therefore be made by either comparing the numeric values of metabolite ratios or recognizing abnormal patterns of resonances in the spectra. With either method, it is the increase or decrease in the ratios of the metabolites that are diagnostic for pathology.[46]

## 2.2. Gray and White Matter

The spectral differences between gray and white brain matter are important, both physiologically and when using the spectra for diagnostic purposes, and are shown in Figure 6, from a healthy person, using both the stimulated echo

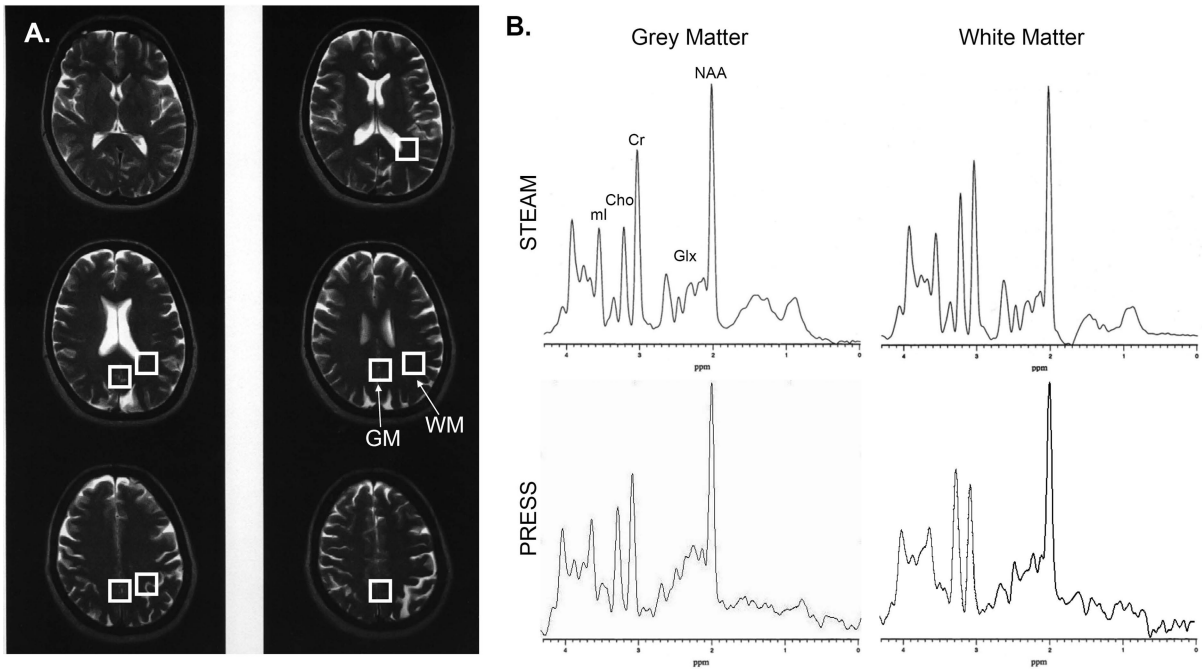


**Figure 6.** Gray vs White Matter of the Human Brain at 1.5 T: (A) Multiple axial $T_2$w MRI slices (5 mm between each slice) showing voxel locations for gray matter (GM) and white matter (WM) voxel locations as indicated. All six slices show the inferior and superior slice locations as defined by the acquisition protocol. Data obtained from B. D. Ross and A. Lin. (B) *In vivo* spectra obtained from each region using STEAM (TE/TR = 30/1500 ms, 256 averages) and PRESS (TE/TR = 35/1500 ms, 128 averages) single voxel spectroscopy localization methods. In both cases, a 2 × 2 × 2 $cm^3$ voxel volume is used. Note that there are subtle differences in the metabolite peak heights depending on which method is used. Data obtained from B.D. Ross and A. Lin.

acquisition mode (STEAM) (section 3.7) and point-resolved spectroscopy (PRESS) (section 3.8) methods. Recognizing these differences in the healthy state is integral for both the diagnosis and biochemical understanding of disease in the brain.

### *2.2.1. Voxel Placement for Examining Gray and White Matter*

The spatial location from where the data is collected is called the "voxel" or the region of interest (ROI). Placement of ROI is an inherent part of collecting spectra of high quality and thus diagnostic quality.

In the clinic, there are two voxel locations that are important for diagnostic purposes both for nonfocal disease and for research purposes. These are the gray matter and white matter. The gray matter voxel location is often referred to, by others, as occipital gray matter or posterior cingulate gyrus and is primarily utilized to assess neuronal health in the human brain. For example, in Alzheimer's disease, the gray matter is a watershed region that is highly sensitive to changes in NAA due to neurodegeneration. Hypoxia, dementias, systemic disease (such as hepatic encephalopathy), and infections (such as HIV) all affect cerebral metabolite levels, especially NAA. The white matter voxel is used to assess axonal condition and is affected by diseases such as multiple sclerosis, leukodystrophies, and many metabolic disorders. By comparison of metabolite ratios from a database of age-matched, normal subjects (Table 1), many diseases can be diagnosed using these two regions alone.

**Table 1. Normative Metabolite Ratios Measured at 1.5 T[a]**

| Left Parietal White Matter (PRESS; TE = 35 ms; TR = 1500 ms; Avg = 128) | | | |
|---|---|---|---|
| Age | NAA | Cho | mI |
| 21−40 | 1.91 | 1.04 | 0.70 |
| 41−65 | 1.66 | 1.01 | 0.75 |
| >65 | 1.66 | 1.11 | 0.73 |
| **Occipital Gray Matter (PRESS; TE = 35 ms; TR = 1500 ms; Avg = 128)** | | | |
| Age | NAA | Cho | mI |
| 21−40 | 1.55 | 0.60 | 0.67 |
| 41−65 | 1.53 | 0.70 | 0.69 |
| >65 | 1.41 | 0.62 | 0.60 |

[a] Reprinted from *NeuroRX*, Vol. 2, Lin et al, Efficacy of proton magnetic resonance spectroscopy in neurological diagnosis and neurotherapeutic decision making, pp 197−214, 2005 with permission from Elsevier.[46]

## *3. Data Collection and Post-Processing*

We consider this to be an important component of this review. It is clear by assessing the literature that there is a wide range of technical methods and variable spectral quality (ranging from outstanding to uninterpretable). The manufacturers have all attempted to automate the acquisition of neurospectroscopy. However it remains common for untrained technologists (Radiographers) to accrue spectra that fail to produce minimally acceptable data. Those sites that reproducibly report high-quality spectra from the brain, usually, have a Ph.D. chemist or physicist driving the scanner. This factor alone has caused the diagnostic capacity of neurospectroscopy to remain site specific.

## 3.1. Optimizing the Signal-to-Noise Ratio

During data collection, the analogue free induction decay (FID) is first filtered using a low pass filter to eliminate high-frequency noise before passing through an analog-to-digital converter (ADC) where it is sampled with a number of digitalization points, $n$, for time duration, $T$, to produce a

digital version of the signal. The time interval ($t$) between two consecutive sampling points is the dwell time. The number of digitalization points, duration of data collection, and dwell time are linked as expressed in 1:

$$t = T/n \quad (1)$$

where $t$ = dwell time, $T$ = acquisition time, and $n$ = number of digitalization points. The Fourier transformation of such a FID is a spectrum having $n$ sampling points at intervals of $1/T$ Hz and a total spectral bandwidth of $n/T$ Hz when using quadrature detection. The digital resolution of the spectrum is $1/T$ and determines the final frequency resolution of the resultant spectrum. Improvements in spectral resolution may be obtained by using longer acquisition times or by increasing the number of data points only if the transverse relaxation of the acquired species is long enough. Acquisition time is usually limited by the decay time of the signal; thus extending the duration time significantly beyond the signal decay time results in the collection of background noise, resulting in degradation of spectral SNR ratio as well as elongation of measurement time. These parameters should be interactively considered to maximize spectral resolution and SNR and therefore the amount of data available for final analysis.

## 3.2. Data Acquisition

In all MRS experiments, the acquisition parameters are adjusted on a scan-by-scan basis to optimize spectral resolution and SNR. The process of automatically adjusting these parameters is referred to as "prescan" and usually involves shimming, power calibrations, and frequency and water suppression adjustment. While all prescan adjustments are important in the acquisition of MR spectroscopy, two parameters hold particular importance (shimming and water suppression) and are crucial to the success of *in vivo* spectroscopy.[47]

## 3.3. Shimming

The line width of a resonance is dependent on the intrinsic transverse relaxation of that resonance as well as the homogeneity of the magnetic field in the localized region under investigation. The combined effect of the intrinsic transverse relaxation plus the effect from magnetic field inhomogeneity produces the observed line width. In biologic tissues, variations in the main magnetic field ($\mathbf{B}_o$) that arise from extrinsic factors cause broadening and distortion of resonance characteristics and must be minimized to acquire successful *in vivo* data. Consequently, when a subject is placed in a MR scanner, significant $\mathbf{B}_o$ inhomogeneities are generated that depend on the presence and distribution of different tissue types. These $\mathbf{B}_o$ inhomogeneities are often the dominant factor limiting MR spectroscopy applications, with *in vivo* spectroscopy being particularly sensitive to even very small variations in magnetic field uniformity.

Shimming is the process by which the $\mathbf{B}_o$ field is made as homogeneous as possible and is usually achieved using the linear $x$-, $y$-, and $z$-gradient coils. Most automated shimming routines acquire a $\mathbf{B}_o$ field map, and the $x$-, $y$-, and $z$-linear gradient coils are adjusted to minimize inhomogeneities.[48,49] The inclusion of higher-order shim coils, capable of generating second- and third-order spherical harmonics, in addition to linear gradient coils has been shown to yield improved results.[50] While autoshim procedures provide reasonable results in the homogeneous surrounds of the brain at lower magnetic field strengths ($\leq$1.5 T), increased magnetic susceptibility shifts in inhomogeneous regions or at higher magnetic field strengths ($\geq$3 T) may require the inclusion of higher-order shim terms in addition to linear terms to obtain high-quality spectroscopic results (Figure 7).

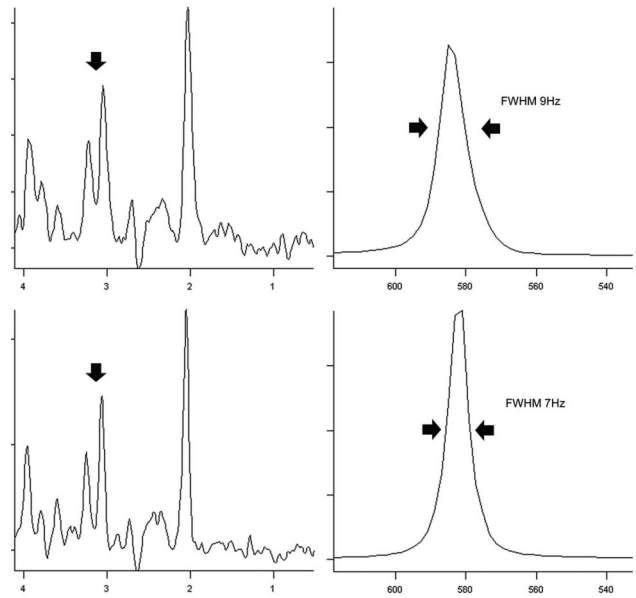


**Figure 7.** Influence of manual shimming. *In vivo* single voxel study of human brain at 3 T; TE 135 ms, TR 2000 ms. Top left: Single voxel spectrum obtained with automated shimming only. Top right: Corresponding water reference acquired with automatic shimming only that demonstrates FWHM of water of 9 Hz. Bottom left: Single voxel spectrum from the same location obtained following manual shimming. Vertical arrow indicates better separation of the choline and creatine resonances compared with the result from automated shimming only (top left panel). Bottom right: Corresponding water reference acquired with additional manual shimming that demonstrates FWHM of water of 7 Hz. Reprinted with permission from Stanwell and Mountford, *RadioGraphics*, 2007, Vol. 27, pp S253−266. Copyright Radiological Society of North America.[155]

## 3.4. Water Suppression

For *in vivo* proton spectroscopy, the water resonance is suppressed to allow for the detection of the metabolite signals of interest, which can be 10 000 times less concentrated than water. Water suppression usually involves the implementation of a series of three variable flip angle[51] or one 90°[52] water frequency selective RF pulses followed by dephasing gradients that result in dephasing of the water signal. Due to finite water relaxation times, water suppression is typically achieved using RF flip angles other than 90° (typically 110°−120°),[51] and thus improved water suppression can be achieved by varying the RF power of the final frequency-selective pulse to enhance suppression of the water signal. Most automated prescan procedures include a step where the RF power is systematically adjusted to achieve optimal water suppression and can usually be manually adjusted to provide an optimal level of suppression.

## 3.5. Localization To Examine an Area of Disease

Localization is needed when examining a specific region involving disease. The data needs to be collected from a well-

defined, spatially dependent ROI while excluding signal from unwanted surrounding tissue. *In vivo* studies generally use ROIs between 3 and 8 $cm^3$; however, with higher magnetic field scanners, ROIs as small as 1 $cm^3$ can be studied (see section 3.1). Nevertheless when the ROI is reduced so is the amount of tissue present within the ROI, and the measurement time must be increased to maintain a consistent SNR. In order to optimize reproducibility, the voxel parameters must be the same in every patient for a specified examination. All other parameters can be set as part of a protocol, leaving voxel position as the only factor that can affect reproducibility. For global diseases, such as Alzheimer's disease or hypoxia, the voxel positions are predetermined, as described in section 2.2.1; however in focal disease, such as brain tumor, voxel position and size can be variable and require careful thought when determining these factors.[53]

Two types of localization methods are commonly used: single voxel spectroscopy (SVS) and chemical shift imaging (CSI).

## 3.6. Single Voxel Spectroscopy (SVS) Methods

These methods all make use of modulated, frequency-selective RF pulses applied in the presence of a pulsed gradient field. To select a volume, three selective pulses are applied, one after the other, in the presence of mutually orthogonal field gradients. The intersection of the three excited planes defines the ROI. Two common approaches used for localization are described and their attributes discussed below.

## 3.7. STEAM ("Stimulated Echo Acquisition Mode")

The sensitive volume in STEAM ("stimulated echo acquisition mode"[23]) localization is selected by three consecutive slice-selective 90° pulses that generate a stimulated echo from the ROI with full localization achieved in a single scan without the need for phase cycling. Advantages of the STEAM technique include well-delineated ROI because the frequency-selective 90° pulses generate a good slice profile, signal losses due to $T_2$-relaxation remaining minor, excellent water suppression, and the 90° RF pulses employed being more broadband than equivalent 180° pulses with the advantage that the resultant localized signal is less dependent on RF inhomogeneities and reduced peak RF power is required. However, STEAM localization suffers from up to 50% signal loss compared with the PRESS technique, which can translate into an up to 26% increased ROI dimension or up to 4-fold increased measuring time.[54]

## 3.8. PRESS ("Point-Resolved Spectroscopy")

The sensitive volume in PRESS ("point-resolved spectroscopy"[55]) localization is selected following the application of a slice-selective 90° pulse followed by two slice-selective 180° pulses that generate a spin echo from the ROI. The principal advantage of PRESS over STEAM localization is the additional SNR gained in the collection of a spin echo over a stimulated echo. This advantage however may be partially reduced if there are significant $T_2$ losses, which are more pronounced in PRESS than in STEAM. PRESS disadvantages also include poor slice profile even if improved pulse designs[56,57] are employed (Figure 8), the transition bands of the RF pulses generating unwanted coherences that need to be eliminated, and increased peak RF power required to retain the same chemical shift displacement error when compared with STEAM localization. Shinnar-Le Roux (SLR) refocusing RF pulses[58] have been proposed as a solution for an accurate slice-selective refocusing pulse but they suffer from long duration.

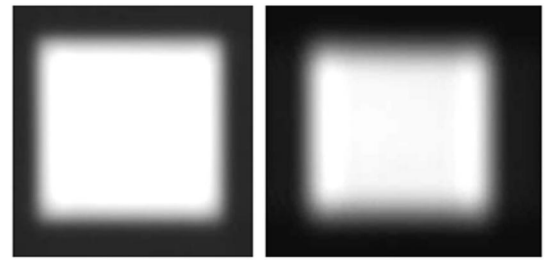

**Figure 8.** Comparison of single voxel localization techniques. (left) Image of the excited volume using the STEAM technique acquired at 1.5 T. (right) Image of the same excited volume using the PRESS technique at 1.5 T. Sharper transitions at the voxel boundaries are apparent with the STEAM technique. Data obtained from P. Stanwell.

## 3.9. Chemical Shift Imaging (CSI)

In experimental duration, some 2−3 times longer than that in which a single voxel method acquires the spectrum of a single ROI, the CSI technique[59] can collect an array of spectra from a single plane. Phase-encoding gradients are employed to encode the spatial dimensions, and the MR signal is collected in the absence of any gradient in order to maintain the spectroscopic information. Each acquired ROI contains a MR spectrum that allows for the assessment of the metabolic profile of a specific location or allows for visualization of the spatial distribution of specific metabolites of interest. CSI also allows for the acquisition of smaller volumes than in single voxel techniques (as small as 0.4 $cm^3$ at higher magnetic field strength).

CSI suffers from the disadvantage that the shape of individual ROIs is less well-defined than that in single voxel techniques. This can result in the adjacent ROIs being contaminated by large amplitude signals from surrounding ROIs. Though typically more time-consuming than single voxel techniques, CSI can examine a larger area of interest than single voxel studies. Efforts to reduce the acquisition time of CSI are under development.[60,61]

## 3.10. Spectral Processing

MR spectroscopy processing typically involves converting the time domain signal (FID) to the frequency domain with quantitative analysis carried out in either the frequency domain,[62] the time domain,[63] or a combination of both.[64] Most data processing focuses on the analysis of signal amplitudes or integrals because these reflect the tissue levels of metabolites. However, the ROI measured by *in vivo* MR spectroscopy normally contains many thousands of cells with varying degrees of heterogeneity as well as blood vessels and other intercellular spaces. The chemical composition will vary according to the cellular or disease composition of the ROI (voxel). Analysis of this data set may be performed in several ways, but the goals of any analytic method are the same: (1) presentation of spectroscopic data in an easily interpretable format; (2) assignment of resonance to specific metabolites; and (3) robust determination of the relative ratios of metabolites.

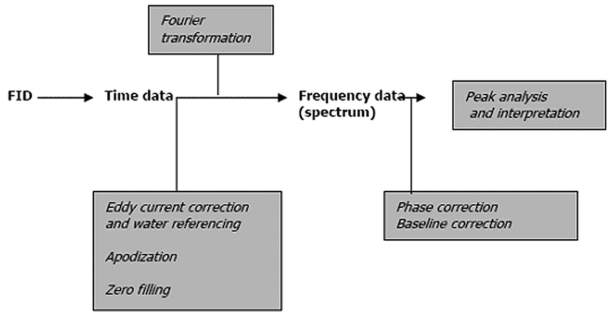


**Figure 9.** Flow scheme from raw time domain data, produced by an MRS experiment, to clinical diagnosis or biomedical interpretation. The raw data can be processed by appropriate software supplied by MR manufacturers or by stand-alone software. The quantitative result can be used either for further interpretation or diagnosis or as input into a pattern recognition routine for eventual classification. Raw time-domain data may also be directly fed to pattern recognition routines for classification. Reprinted with permission from Stanwell and Mountford, *RadioGraphics*, 2007, Vol. 27, pp S253−266. Copyright Radiological Society of North America.[155]

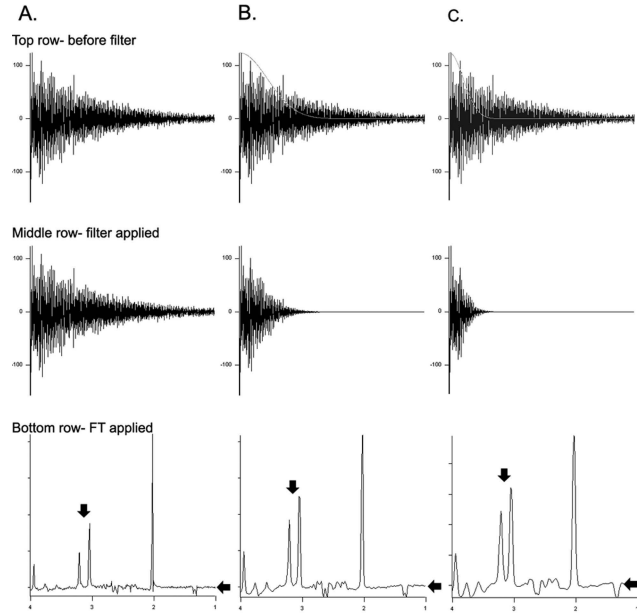


**Figure 10.** Effect of time domain apodization. The top row demonstrates the same FID collected from a brain phantom at 3 T (TE 135 ms, TR 2000 ms). The filter is shown overlaid on the FID (exponential delay curve) but not yet applied: (A) no filter; (B) 300 ms filter; (C) 150 ms (not yet applied). The middle row demonstrates the effect of applied filter function on the FID. The bottom row demonstrates the final spectrum following Fourier transformation. Signal-to-noise improves from left to right (e.g., 0−1 ppm range; A−C), while spectral resolution decreases from left to right (e.g., lactate doublet 1.31 ppm; A−C). Reprinted with permission from Stanwell and Mountford, *RadioGraphics*, 2007, Vol. 27, pp S253−266. Copyright Radiological Society of North America.[155]

## 3.11. Preprocessing

The FID is a time domain signal that consists of the superposition of several signals that evolve at different frequencies and decay with different time constants. While analysis of the FID itself can be done, it is more common to process the FID following Fourier transformation. Fourier transformation converts the time domain signal to a frequency domain signal. This frequency domain signal is a display of absorption peaks occurring at the various frequencies that contribute to the signal (Figure 9).

While any of the MR signal processing manipulations may be performed prior to or following Fourier transformation, certain operations are computationally easier on one or the other form of the signal. The processing steps that are usually applied to the time domain signal consist of water referencing, apodization, and zero filling (see Figure 9). Other optional processing steps performed in the time domain are corrections for spectral distortions from residual eddy currents and the removal of the water peak. Following Fourier transformation, phase correction, baseline correction, and curve fitting (including quantification) are performed on the frequency domain spectrum.

## 3.12. Eddy Current Correction and Water Referencing

Rapid switching of gradient magnetic fields produces electric currents known as eddy currents in conducting structures surrounding the magnet (e.g., cryogenic shields). Most modern scanners are equipped with actively shielded gradients that minimize eddy currents.

## 3.13. Water Referencing

Temporal or spatially dependent experimental artifacts, which are difficult to assess from metabolites with low SNR, can be corrected using the much stronger signal of water. This signal can be obtained from the same ROI (e.g., acquiring a separate measurement using no water signal suppression). Additionally, frequency shift corrections using either the water or another major signal as a reference can be used to correct for frequency variations between ROIs in CSI[5] or in spectra obtained as a function of time.[65]

## 3.14. Water Subtraction

Water subtraction is also undertaken in the time domain to reduce its influence on metabolites close to the water resonance. This is usually achieved by low-frequency filtering.

## 3.15. Apodization

Apodization is the multiplication of the raw MR time domain signal by a particular function with the intention of (1) improving SNR, (2) improving spectral resolution, (3) removing truncation artifacts (Figure 11), or (4) removing broad spectral components in the frequency domain.[66] In *in vivo* MR spectroscopy, the most common filter functions decay with time, so the signal is enhanced at the beginning of the data collection period and is suppressed at the end. This improves SNR at the expense of some broadening of the spectral signals (see Figure 10). For optimal signal enhancement, the decay time of a filter should be matched to the decay time of the FID. A filter that decays much slower than the signal is referred to as a weak filter and does not have a noticeable effect on the spectrum. A filter that decays considerably faster than the signal is a strong filter. It causes extreme broadening of the spectral peaks with loss in spectral resolution and in signal intensities.

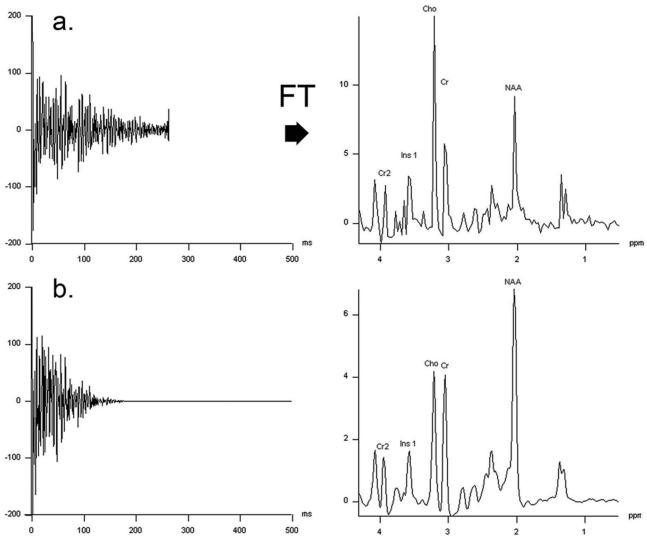


**Figure 11.** Truncation artifact. The top row demonstrates truncation of a FID collected from a brain phantom at 3 T (TE 30 ms, TR 2000 ms) by making the collection time too short, resulting in abnormal depiction of resonance amplitudes (e.g., NAA at 2.02 ppm, choline at 3.21 ppm). The bottom row shows apodization of the truncated FID with a decaying function that results in smooth decay of the FID. Following Fourier transformation, the resonance amplitudes return to an expected result, at the expense of decreased spectral resolution. Data obtained from P. Stanwell and C. Mountford.

## 3.16. Zero Filling

Spectral bandwidth, BW, is equal to the number of digitization points, *n,* divided by the data collection time, *T*.

$$\mathrm{BW} = n/T \tag{2}$$

For most MRS measurements, the spectral BW is specific to each nucleus and is determined by the range of frequencies contained in the signal. Thus receiver bandwidth should be kept wide enough to detect all spectral frequencies but narrow enough to minimize noise contribution to the signal, and data collection time should be long enough to collect signals from the beginning of the FID but short enough to avoid collecting background noise from the end of the FID. Therefore the number of digitization points of the time domain signal cannot be increased arbitrarily in order to increase the spectral resolution.

Zero filling is a method of artificially increasing the number of digitization points by inserting additional data points of zero amplitude at the end of the FID following data acquisition. The spectral resolution is improved in this manner producing a better representation of fine details and allowing a more accurate definition of the position and height of peaks.[67]

## 3.17. Phase Correction

During a spectroscopy measurement, phase shifts may be introduced as a result of hardware settings or sequence timing, which produces frequency-dependent phase shifts. Following Fourier transformation, these shifts introduce a mixture of absorption and dispersion signals into the frequency spectrum. Since quantitative analysis is performed on a pure absorption spectrum, a phase correction procedure is required in order to separate pure absorption and pure dispersion modes into the real and imaginary parts of the complex spectrum. Most phase shifts encountered in *in vivo* proton spectroscopy may be corrected with a constant or zero-order phase factor. Automatic, unbiased zero-order phase correction of proton MR spectra is achieved by the point-wise division in the time domain of the phase of the measured signal using a water reference for correction.

## 3.18. Baseline Correction

The baseline of a MR spectrum should ideally be flat until the resonance peak is reached. However there are several factors that limit this occurrence even after appropriate phase correction. This distortion is more apparent in CSI sequences where time is allowed for phase encoding before collecting the spectral data. Other frequent baseline distortions include broad spectral humps due to macromolecules with short $T_2$ relaxation and baseline sloping caused by the edges of the water resonance when water is not subtracted during post-processing, which is more apparent at short echo times.[41] Most processing packages have the capability of estimating the baseline using spline or polynomial functions and can correct baseline distortions by subtracting the estimated distortion from the original spectrum.

## 3.19. Methods of Spectral Analysis

*In vivo* proton MR spectra from the brain consist of numerous overlapping biochemical signals, many with low signal amplitude. The area under a resonance, or a composite resonance, relates to the amount of the corresponding metabolite that is mobile on the MR time scale. However, measuring the individual resonances is a time-consuming undertaking revealing only a small percentage of the information available and requiring significant operator input with the results often becoming operator dependent. Additionally, this approach is challenged when studying overlapping resonances (e.g., glycine and myoinositol) or when studying resonances with complex *J*-coupling (e.g., glutamate and glutamine). Identifying signal differences in this situation can be significantly improved by incorporating prior knowledge into spectral processing.[68,69] Alternatively, pattern recognition methods can be invoked to aid class distinction within large data sets (30 or more in each category).[70,71]

### *3.19.1. Prior Knowledge*

The incorporation of prior knowledge models into spectral processing is commonly undertaken as part of specialized spectral processing software packages that incorporate the usual processing steps (e.g., apodization, zero filling, phase correction, etc.) but additionally incorporates prior knowledge of the expected metabolites. The two most common approaches accomplish this in either the time domain or frequency domain. Theoretically, there is little difference between analyses undertaken in the two domains; however there are advantages and disadvantages to both categories. Time domain methods avoid preprocessing of the measured signal, whereas frequency domain methods process the Fourier transformed original signal. Time domain methods have the advantage of easily managing missing data points[72] as well as affording greater flexibility to the model function adopted in contrast to frequency domain methods.[73] Frequency domain methods have the advantage of being naturally suited to frequency selective analysis, which can reduce the number of model parameters, hence requiring less computational demands.[73]

Time-domain routines are typically divided into two different approaches: interactive and noninteractive. Noninteractive approaches, in general, attempt to minimize the difference between data and the model function using local or global optimization theory.[74] Interactive approaches tend to make use of a basis set of metabolite profiles. Magnetic resonance user interface (MRUI)[75,76] is a commonly used time-domain method that utilizes two approaches for "quantitation", AMARES (advanced method for accurate, robust, and efficient spectral fitting)[77] and QUEST (quantitation based on quantum estimation).[78] AMARES is an interactive time-domain method that attempts to fit a parametrized model function to the data by minimizing a cost function.[77] QUEST involves fitting the measured MR signal with a sum of adjusted spectra acquired either from metabolites of interest in solution under the same experimental conditions in which *in vivo* spectra are to be obtained or by creating a simulated metabolite basis set built up from simulated spectra based on quantum mechanics.[78]

Frequency domain quantitation routines operate by examining the area under resonances of interest and the incorporation of model line shape methods.[62] LCModel is a commonly used frequency-domain method that involves fitting the measured MR signal with adjusted, complete model spectra derived from an *in vitro* basis set acquired from metabolites of interest in solution.[62] A linear combination of these spectra is then used to fit the *in vivo* data in the frequency domain and to estimate metabolite levels. A constrained regularization method accounts for disparity in phase, baseline, and line shapes between the *in vitro* and *in vivo* spectra.[79]

Interactive methods like AMARES work best in the setting of well-separated peaks and are less appropriate for complex signals such as short TE spectra, where peaks with large amplitudes are in close proximity to peaks with small amplitude. In this setting, QUEST and LCModel are better suited because more prior knowledge is included in the formation of metabolite basis sets, particularly with respect to the experimental conditions of acquisition.[74] However when prior knowledge is added, it is important to incorporate the actual acquisition parameters including the applied external magnetic field strength, temperature, echo time, repetition time, pH, and pulse sequence used for acquisition. Additionally, since the metabolite basis set is invariably generated from a set of *in vitro* samples, even if the utmost care taken to acquire the *in vitro* signals with the exact same MR parameters that are intended for use *in vivo*, the final values need to be screened for their biological relevance. Also, for accurate "quantitation", the relative amounts of macromolecular signals should be included in the prior knowledge model when macromolecular contributions are expected in the *in vivo* spectrum.[74]

The wavelet transform is yet another method used for spectral processing. The wavelet transform has several advantages compared with the traditional Fourier transformation including increased stability to small perturbations of signal (e.g., those encountered in difficult baselines or in the presence of significant local field inhomogeneities).[80] The wavelet transform decomposes a signal into both time and frequency representations of the original signal leading to better representation of signal components. As such, wavelet transforms have found several applications in MR spectral processing including signal subtraction,[81] baseline removal,[82] and denoising of spectra with low SNR.[80,83] Apart from applications to signal processing, the wavelet transform has also been applied to quantitation[84,85] and automated methods of spectra classification.[86,87]

### 3.19.2. Pattern Recognition Systems (PRS)

Pattern recognition blends pattern recognition techniques and multivariate statistical analysis with solid, comprehensive software engineering practices.[71] To overcome the shortcomings in the aforementioned prior knowledge approaches, the use of computer-based methods, so-called pattern recognition methods, have been advocated.[71,88,89] Such methods in no way rely on prior information but do require a larger number of data sets to be produced in order for robust classifiers to be developed. There are many advantages to the pattern recognition methods. They allow for the detection of subtle differences in metabolic profiles and, in some instances, for the identification of biomarkers of disease.

Pattern recognition methods are undertaken following preprocessing of data and can be divided into two classes: unsupervised and supervised methods. Unsupervised methods usually involve some form of data complexity reduction so that the inherent clusters in the samples can be visualized, leading to the selection of the descriptors, which are important for the clustering.[88] The group membership of each sample is then compared with an independent but known outcome (e.g., histopathology or clinical diagnosis) to check the final validity of the PRS method. Supervised methods involve first a training set of data in which the outcomes are known (e.g., histopathology or clinical diagnosis) and that can be used to construct a mathematical model based on the input descriptors.[88] The classifier developed using the training set is then applied to the test set and the validity of the classifier is checked by comparison with the known diagnosis of the test set. The choice of classification method is largely determined by the distribution (e.g., normal distribution) and the degree of variance of data being examined.

The pattern recognition method does however require a larger database in order to generate robust classifiers. This latter method has been successfully used by several of the authors.[90] It offers the opportunity for a totally independent diagnosis of a clinical MRS data set where the MR spectra are compared with extensive clinic pathological databases for each patient. An example of this method applied to neurospectroscopy from patients with chronic pain is described below (section 6.3).

### 3.19.3. Decision Support System (DSS)

A computer-based decision support system to assist radiologists in diagnosing and grading brain tumors has been developed by the multicenter INTERPRET project.[91] Spectra from brain tumors from 334 patients at four different centers were clustered according to pathology using pattern recognition techniques. The results are presented as a two-dimensional scatter plot using an intuitive graphical user interface.

The prototype decision support system classified 89% of the cases in an independent test set of 91 cases for the most frequent tumor types (meningiomas, low-grade gliomas and high-grade malignant tumors, glioblastomas, and metastases) (Figure 12). The method also assisted in the correct diagnosis of cases that were difficult. The philosophy behind this development was that in the immediate future a diagnostic

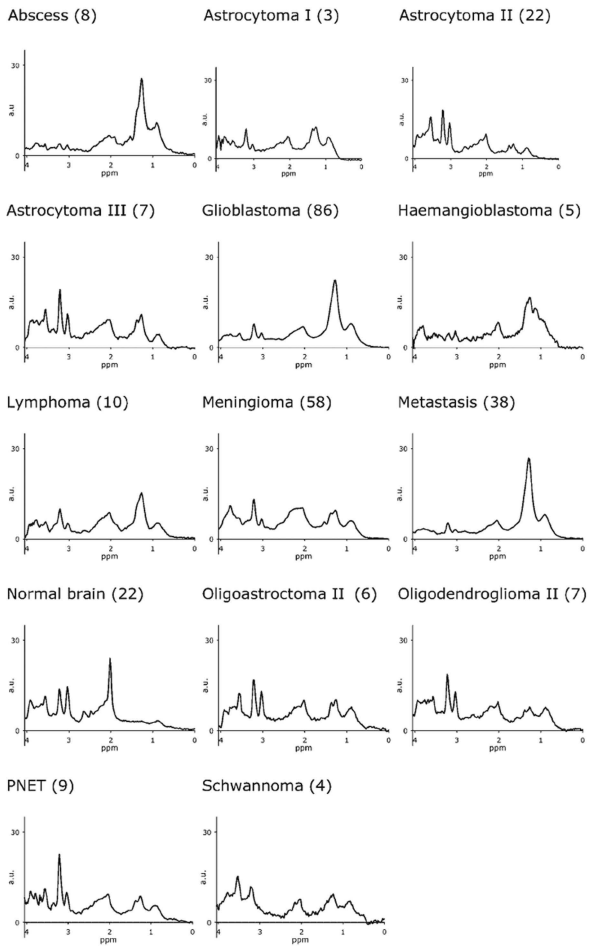


**Figure 12.** Decision support system. These are the mean short echo proton MRS spectra, 1.5 T, of representative pathologies obtained as part of a multisite study. They were obtained by averaging spectra normalized to the Euclidian norm. The vertical axis is displayed in the same arbitrary units scale for all types. The horizontal axis labels ppm values. Number of cases of each type in parentheses. The most relevant metabolites are lipids (0.9 and 1.29 ppm), lactate (doublet centered at 1.33 ppm), alanine (doublet centered at 1.47 ppm), *N*-acetyl-containing compounds (2.03 ppm), acetate (1.9 ppm), macromolecules and glutamate/glutamine-containing compounds (2−2.5 ppm), creatine (3.03 ppm), choline-containing compounds (3.21 ppm), myoinositol and glycine (3.55 ppm), and glutamate/glutamine-containing compounds and alanine (3.77 ppm). Reprinted with permission from ref 92. Copyright 2006 Wiley-Blackwell.

algorithm will be used as one factor among many when a clinical diagnosis is being made.

The authors report that when a prototype was tested by radiologists and other clinicians, it was favorably received and the preliminary clinical analysis of the added value of the INTERPRET DSS for brain tumor diagnosis with MRS showed a statistically significant improvement over MRI used alone.[92]

The INTERPRET DSS[92] was designed to facilitate the incorporation of pattern recognition results into an overall diagnostic procedure *without* requiring blind acceptance of the result of a mathematical algorithm by the clinician. It is interesting to note that in undertaking the research for this review, the acceptance and implementation of the MRS technology (as determined by the paper stating how the results were used clinically) was freely used in countries where litigation is uncommon.

## *4. Spectroscopy in the Clinic*

### 4.1. Outcome for Patients in a Coma

An important aspect of MRS is its capacity to provide a biochemical "window" into the human brain. A prime example is when a patient is in a coma (Figure 13). The current standard of diagnosis is with EEG or clinical psychological tests such as the Glasgow Coma scale, both of which are very crude measurements of brain activity. The capacity to directly measure the number of functioning neurons by MRS is diagnostically important with a clinical outcome to support the usefulness of the method (Figure 13).[93] An outcome index (SPI) that uses all of the observed neurochemical measures in the spectrum was effective.[94]

In coma cases when NAA is reduced by 10% or less compared with normal healthy brain, the outcome is generally good with partial to full recovery of neurological functions. With a reduction of 20−40%, the prognosis is less good shading into a condition defined as persistent vegetative state. This implies that the patient may awaken but not be neurologically functional or may never recover consciousness. When there is a loss of more than half of the NAA signal this implies permanent coma status or death.[94] To add additional specificity to this test in cases where brain damage may be a result of hypoxia (when coma status is a result of lack of oxygen to the brain due to suffocation or lack of blood flow), lactate appears in high concentrations in the brain as a result of anaerobic (lack of oxygen) metabolism.[95] Physicians can then make informed decisions about patient management. Often when spectral NAA is severely reduced in intensity, the decision will be made to allow the patient to pass away peacefully as opposed to further medical procedures. This has the potential to save significant funds in healthcare costs and provides an objective assessment to assist the family in the decision-making process.[96]

In one example from the USA, ventilator support was terminated with the approval of the institutional review board (IRB) when neurospectroscopy findings, clinical neurology, and EEG all concurred in predicting vegetative outcome following near-drowning. In Australia, the family of a young man in a coma was considering terminating ventilator support

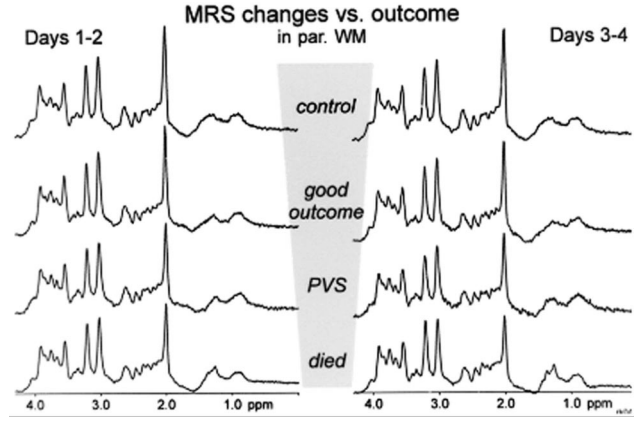


**Figure 13.** Coma. STEAM spectra of comatose patients. Spectra of four different patients that were in a coma on days 1−2 (left) and days 3−4 (right). Outcome of the patient is indicated in the middle slice. Note the presence of lactate in the bottom right spectrum. Otherwise, the only difference between each coma outcome was the NAA resonance at 2.03 ppm. NAA peak height therefore directly correlates with patient outcome. Data obtained from B.D. Ross and A. Lin.

following a motor bike accident. When the neurospectroscopy examination showed a healthy brain spectrum, the decision was reversed. The young man awoke several weeks later. There are similar reports by Ashwal et al. and Kadri and colleagues.[96,97]

## 4.2. Hypoxic Brain Injury

The MRS profile of hypoxia[93] is as well documented now as brain tumors.[98] The following are representative cases and cover many of the major questions asked when applying proton neurospectroscopy in clinical practice. There are two cases, shown in Figure 14, where neurospectroscopy was requested by the neonatologist after a neurologist suggested severe hypoxic brain injury with a guarded prognosis. The protocol (PRESS TE 35 ms; voxel size 8 $cm^3$) and ROI (in the water-shed area of gray matter in the future posterior cingulate gyrus) was used for each infant. These two spectra were adequate to provide prognostic information at the first neurospectroscopy examination. Infant 1 was comatose when examined on Day 1, but the neurological outcome was excellent, and the child was alert when examined again by neurospectroscopy on Day 4 (not shown). Infant 2 was examined in coma on Day 5 and again on Day 35 (not shown). The presence of lipid and lactate, as well as decreased NAA/Cr, distinguished infant 2 from infant 1. For a control spectra from healthy infants, see Danielson and Ross.[24]

A review of the literature[99] identified 137 articles, reviews, and full-length abstracts that use long-echo time, short-echo time, or chemical shift imaging proton spectroscopy to study hypoxia. Of these, 20 studies using the same methodology and, covering 459 total patients, found a correlation between results of MRS performed shortly after hypoxic insult (1−20 days) and neurological or neurodevelopmental outcome at 1 year after the injury.

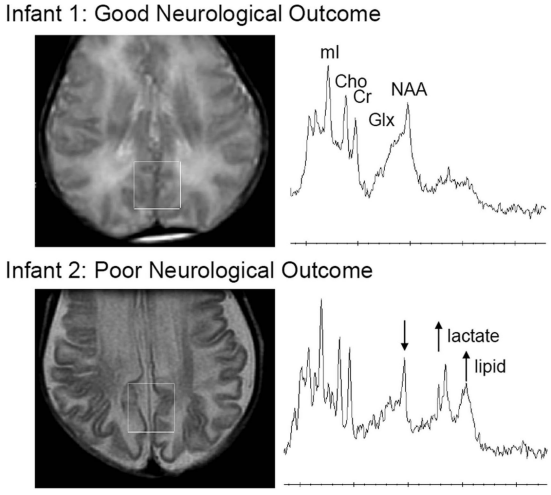


**Figure 14.** Pediatric Hypoxia. Top (Infant 1): (left) MRI shows gray matter MRS voxel location; (right) PRESS (TE = 35 ms, TR = 1500 ms, 8 $cm^3$ volume) spectrum shows relatively normal levels of metabolites. As a result, the infant presented with good neurological outcome despite the hypoxic insult. Note that in infants, NAA starts low and Cho and mI start high. With age, NAA increases and Cho and mI decrease to levels observed in Figure 6 by age 3. Bottom (Infant 2): (left) MRI shows gray matter MRS voxel location; (right) PRESS (TE = 35 ms, TR = 1500 ms, 8 $cm^3$ volume) spectrum shows decreased NAA compared with the first infant and dramatically higher lactate and lipid. As a result, there was poor neurological outcome for this patient. Figure from *Clinical MR Neuroimaging: Diffusion, Perfusion and Spectroscopy* edited by Jonathan H. Gillard, Adam D. Waldman, and Peter B. Barker. Copyright 2005 Cambridge University Press. Reprinted with permission.[93]

## 4.3. Lesions in the Brain

Currently available radiological methods have difficulty distinguishing the many types of brain tumors and an even greater number of species of fungi, bacteria, and parasites. It is normal to obtain a biopsy, either by stereotactic guidance or intraoperatively for those patients who undergo surgery for cytoreduction and decompression. There are significant risks from both surgery and biopsy with a morbidity rate between 2.4−3.5%.[100,101] The biopsy, obtained by either method, will be examined by a skilled neuropathologist to identify the tumor type and if malignant the grade (extent of malignancy) or if an abscess it will be cultured to determine the type and species of the fungus or bacterium.

A noninvasive method for accurate preoperative and prebiopsy diagnosis of brain lesions would be advantageous in almost all cases. This is particularly true where the lesion is a lymphoma or abscess (fungi, bacteria, or parasites) where a preoperative noninvasive diagnosis would negate the need for biopsy and in most cases surgery. The distinction between tumor and abscess is medically important since treatments for abscesses can be as simple as taking antibiotics as opposed to invasive surgery for tumor resection.

### *4.3.1. Abscess*

An abscess is a collection of pus (dead neutrophils) that has accumulated following an infection (caused by bacteria, parasites, fungi, prions, etc.). This mechanism is considered a defensive reaction of the tissue to prevent the spread of infectious material to other parts of the body. The organisms or foreign materials kill the local cells, resulting in the release of cytokines. The cytokines trigger an inflammatory response, which draws large numbers of white blood cells to the area and increases the regional blood flow. As a consequence an abscess generates an MR spectrum containing a variety of metabolites. The resultant spectrum will exhibit resonances that are characteristic of the fungus's, bacteria's, or parasite's own intermediary metabolism (acetate, branched chain amino acids, succinate, etc).

### *4.3.2. Streptococcus milleri*

Streptococcus milleri (Strep milleri) is a name applied to a group of streptococci, which, although basically similar, show various physiological characteristics. Strep milleri have been implicated as etiologic agents in a variety of serious purulent infections and because of their heterogeneous characteristics they may be unrecognized or misidentified by clinical laboratories.

At the bottom of Figure 15, the *in vivo* spectrum (1.5 T, STEAM, TE 20 ms) from a patient with an abscess in the brain is shown. This is compared with the spectra (8.5 T, *in vitro*) from biopsy specimens taken from the brain and liver of the same patient. Then for further comparison, one biopsy was cultured, and the resultant spectrum (top) was compared. The spectra all contain lactate and lipid. The laboratory found all specimens to be Strep milleri. Thus the *in vivo* spectrum recorded from the brain lesion is directly comparable with those obtained from biopsy.

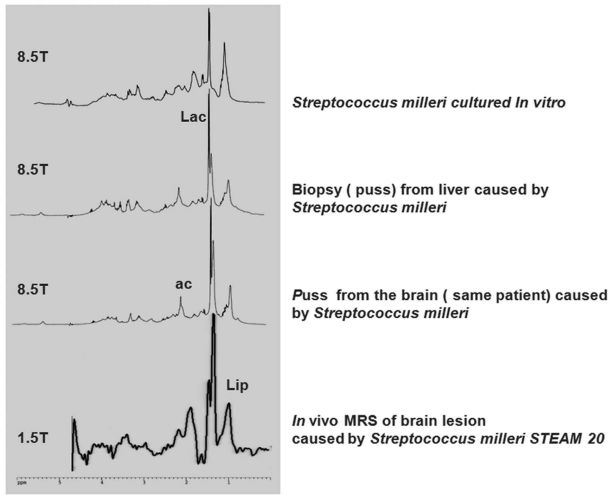


**Figure 15.** Cerebral abscess. MR spectra obtained from a patient with an abcess found to be Streptococcus milleri. On the bottom is the *in vivo* spectrum (1.5 T, STEAM, TE 20 ms) from a patient with an abscess in the brain. This is compared with the spectra (8.5 T, *in vitro*) from biopsy specimens taken from the brain and liver of the same patient. One of these biopsies was cultured, and the spectrum (top) is compared. The spectra all contain lactate and lipid. The laboratory found all specimens to be Strep milleri. Thus the *in vivo* spectrum recorded from the brain lesion is directly comparable with those obtained from the biopsy specimens. Reprinted with permission from Dzendrowskyj, T. E., Ph.D. Thesis, University of Sydney.[156]

The Gupta group, in India, demonstrated that it is possible to distinguish anaerobic from aerobic or sterile brain abscesses on the basis of metabolite patterns observed by *in vivo* proton MR spectroscopy.[102] They showed that etiologic categorization was possible using *in vivo* MRS of a cerebral abscess and verified the findings with spectroscopy on biopsy (Figure 16). In the 1.5 T *in vivo* spectrum, there are resonances assigned from succinate (2.4 ppm), acetate (1.9 ppm), and lactate (1.33 ppm). At the higher field magnetic strength, the biopsy specimens showed lipid at 0.90 and 1.30 ppm, the glutamate−glutamine complex (Glx) at 2.09−2.36 ppm, lysine at 3.01 ppm, taurine at 3.26 and 3.42 ppm, and glycine at 3.56 ppm. The inset data (in panel c) show the expanded region from 3.50 to 3.75 ppm, highlighting the presence of resonances from valine at 3.62 ppm and isoleucine at 3.67 ppm. They then used two-dimensional correlation MR spectroscopy to unambiguously assign the resonances (Figure 16d).

### 4.3.3. Parasitic Disease

A parasite can remain in the body for life, often in an "inactive" form that will not cause any side effects or harm. The infection can be reactivated, however, if the immune system becomes compromised. Two examples of parasitic disease identified by neurospectroscopy are toxoplasmosis (Uwe Himmelreich, Tania Sorrell and Lavia Gomes Unpublished data) and neurocysticercosis.[103]

**4.3.3.1. Toxoplasmosis.** An *in vivo* spectrum reordered from a patient with toxoplasmosis is shown in Figure 17. On the left, it can be seen that the resonances from the methylene and methyl resonance of lipid, at 1.3 and 0.9 ppm, respectively, are prominent. The severely reduced level of NAA indicates the reduction of neurons. On the right is the spectrum from the same patient recorded six months later following therapy, where the NAA, choline, and creatine have now increased indicating that the brain is healing.

**4.3.3.2. Cysticercosis.** The main cause of human cysticercosis is the larval form of *Taenia solium* (pork tapeworm), and a case is shown in Figure 18.[103] The NAA is reduced in intensity indicating lack of neurons. Lactate is normally absent in the brain except in small amounts found in the ventricles. Lactate accumulates in cysts and necrotic tissues and is found in pathologic processes that undergo anaerobic metabolism. Elevated levels of threonine have been demonstrated in cysticercus fluid previously.[104] Elevated levels of lactate and alanine have been demonstrated in abscesses and cysticercosis. Chen et al.[105] demonstrated 18 different amino acids in the cyst fluid of cysticercus, of which alanine and threonine were significantly elevated in neurocysticerci. The peak at 2.4 ppm represents succinate, which is known to be elevated in abscesses and cysticerci.[104] On reexamination, following treatment, lactate, alanine, and succinate peaks decreased and later disappeared. There was recovery of Cr and NAA peaks as the lesion became smaller and more brain tissue was included in the voxel.

### 4.3.4. Tumors

Proton MRS has been shown by many groups to be effective for preoperative and noninvasive diagnosis of brain tumors. MRS is performed in clinical practice to guide the neurosurgeon into the most aggressive part of the lesions and to assist the surgeon in ensuring that the entire tumor is removed. Since the literature is extensive, we have chosen specific examples to illustrate the MRS method. For a systematic review of the literature in this area, see Hollingworth et al.[98]

**4.3.4.1. General Criteria for Diagnosis of Brain Tumors.** It is recognized that for most brain tumors the choline resonance at 3.21 ppm is more intense than the creatine resonance at 3.02 ppm. Then there are additional diagnostic markers for each type of tumor. Tumors are categorized according to the grade or stage of the tumor as described by the World Health Organization. Low grade gliomas, for example, are benign and provide a good prognosis for patients. In contrast, high grade gliomas are considered malignant or highly aggressive where the last stage, stage 4 glioma, has a zero percent survival rate and an average survival of 12 months of life. Neurospectroscopy plays an important role in patient management by distinguishing low grade tumors from high grade tumors. The following are markers for malignancy:

1. Low or absent NAA: As a putative marker for neurons, it would be expected that NAA would be lower when compared with normal brain tissue since brain tumors destroy neurons in the region of the brain that they occupy.[24]
2. Lowered Cr: Creatine is found to be low in certain types of tumors such as pilocytic astrocytomas; however there is often a presence of creatine in most tumors.[106]
3. Elevated Cho: It is thought that the increase in choline is due to accumulation of free choline in the necrotic tissue of tumors and membrane degradation that releases the previously bound choline. Choline is currently the most diagnostic marker for a tumor; however it is important to note that increased choline alone is not specific to brain tumors and that a combination of metabolic changes must be observed to confirm the diagnosis.[24,107]

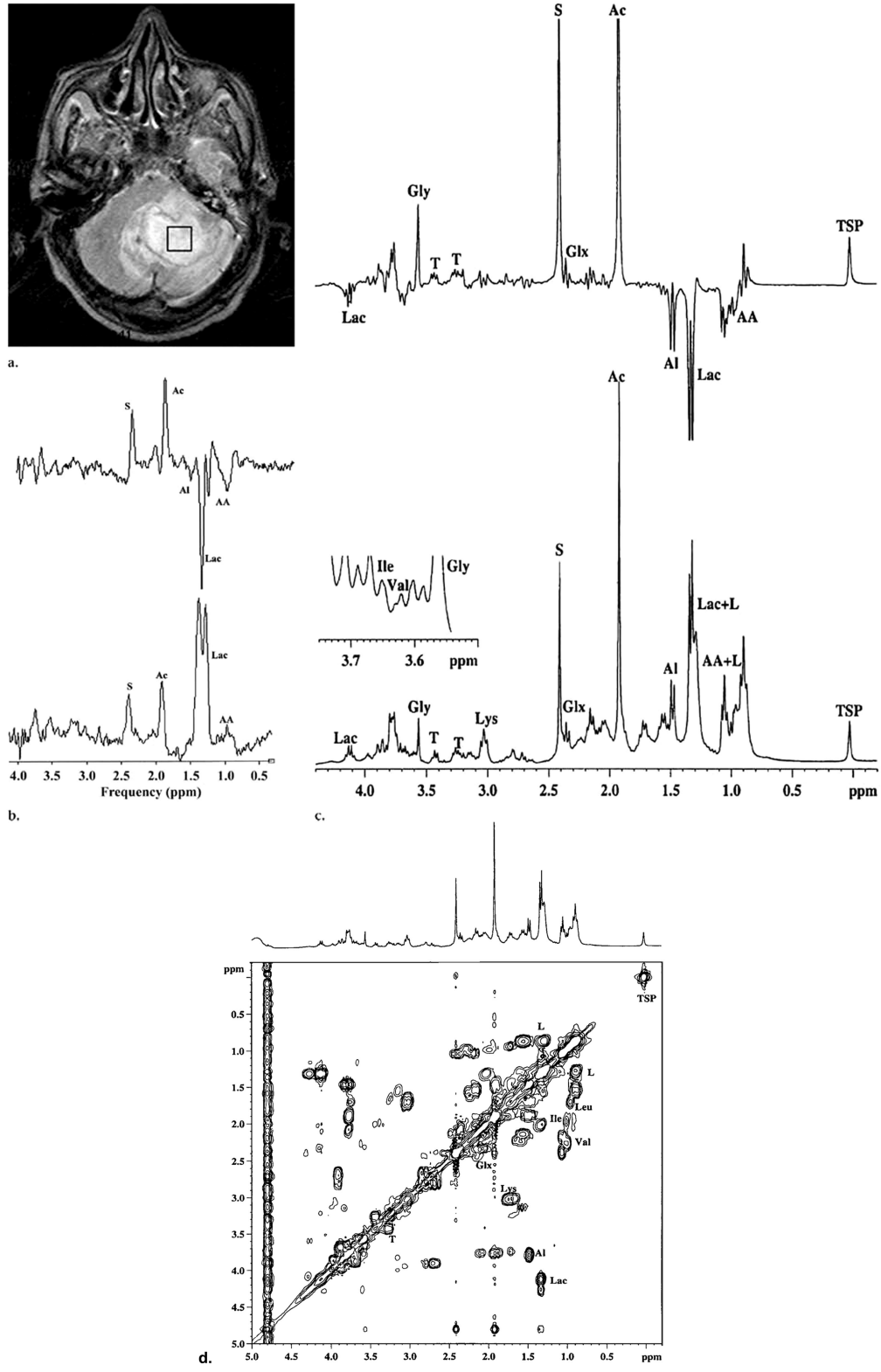


**Figure 16.** Cerebral abscess: (a) $T_2$-weighted MR image (2,200/80) and (b,c) proton MR spectra obtained in patient with cerebellar abscess secondary to *Bacteroides fragilis* group infection. (a) MR image shows the abscess as a hyperintense core in the left hemisphere with a hypointense rim and the location of the MR spectroscopic voxel (box). (b) bottom, *in vivo* proton MR STEAM spectra (3,000/20, 30 ms mixing time) show signal resonances of AA at 0.90 ppm, Lac at 1.33 ppm, Ac at 1.92 ppm, and Suc (S) at 2.40 ppm; top, spin−echo MR spectra (3,000/135) for resonances of AA, Lac, and alanine (Al, at 1.47 ppm) signals show phase reversal that is suggestive of *J* coupling; (c) bottom, data from ex vivo one-dimensional proton MR spectroscopy with single-pulse experiment of the pus show TSP (at 0.0 ppm) as an external reference and signal resonances of lipid (L) at 0.90 and 1.30 ppm, the glutamate−glutamine complex (Glx) at 2.09−2.36 ppm, lysine (Lys) at 3.01 ppm, taurine (T) at 3.26 and 3.42 ppm, and glycine (Gly) at 3.56 ppm in addition to *in vivo* signal resonances—inset data show the expanded region from 3.50 to 3.75 ppm, highlighting the signal resonances of valine (Val) at 3.62 ppm and isoleucine (Ile) at 3.67 ppm; top, on the spin−echo spectrum, signal resonances of AA, Lac, and alanine have inverted. (d) Leucine (Leu, at 1.7 ppm), along with the metabolites seen on the one-dimensional spectra in panel c, all resonances are clearly assigned at ex vivo two-dimensional correlation MR spectrum of the pus. Reprinted with permission from Garg et al, *Radiology*, 2004, Vol. 230, pp 519−527. Copyright Radiological Society of North America.[102]

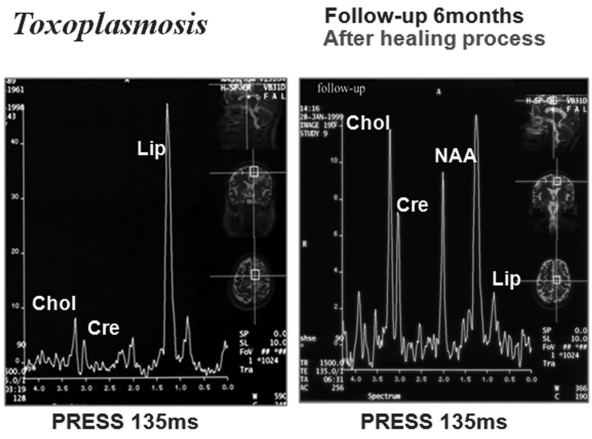


**Figure 17.** Parasitic disease: toxoplasmosis. A single voxel examination (PRESS 135 ms) recorded at 1.5 T from a patient with toxoplasmosis. Left recorded prior to treatment; right 6 months later following treatment. Data obtained from Uwe Himmelreich, Tania Sorrell, and Lavia Gomes.

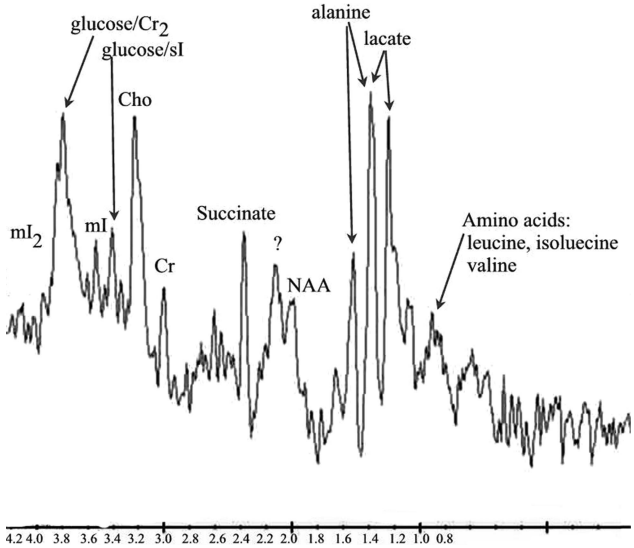


**Figure 18.** Parasitic disease: cysticercosis. A 1.5 T proton brain examination (PROBE) point-resolved spectroscopic sequence (PRESS) short TE (TR 1500 ms, TE 30 ms) MRS sequence shows peaks of metabolites. NAA, *N*-acetylaspartate; Cr, creatine; Cho, choline; Cr2, second creatine resonance; mI, myoinositol. Reprinted with permission from Pandit, S.; Lin, A.; Gahbauer, H.; Libertin, C. R.; Erdogan, B. MR spectroscopy in neurocysticercosis. *J. Comput. Assisted Tomogr.* **2001**, *26* (6), 950−952. Copyright 2001 by Wolters Kluwer Health.[157]

4. Lactate present or absent: Lactate is thought to arise in tumors from anaerobic glycolysis such that highly aggressive tumors are more likely to have increased lactate.[108]
5. Notable excess of lipid: Lipid arises from mobile lipids that are the result of cellular proliferation and degradation and necrosis.[109]
6. Elevated mI is a marker of low-grade tumor.[110]
7. Excess alanine is considered to be a marker of meningioma.[70] In Table 2[111] is summarized the major proton MRS metabolites with peak assignments, detection at short and long echo times (TE), and role (marker).

Large, multicenter studies have shown that MRS can accurately distinguish among different types of brain tumors[92] (Figure 12). The method can also distinguish other brain lesions that can mimic tumors on MRI such as abscesses and lymphomas (see section 3.19.3).

**4.3.4.2. Gliomas.** Gliomas are tumors of the brain that result from mutations in the glial cells that provide structural support for neurons in the brain. There are different types of tumors depending on the type of glial cells from which they originate. For example, astrocytomas originate from astrocytic cells whereas oligodendrogliomas originate from mutations of oligodendrocyte cells. An example of a glioma, recorded from a 32 year old male, is seen in Figure 19. The imaging study (3 T) revealed a large lesion with minimal contrast enhancement and the following spectroscopy study allowed the metabolite maps, NAA/Cr, Cho/Cr, and Cho/NA ratios, to be overlaid on an ADC imaging map (panels A−C). The region of low NAA/Cr and high Cho/Cr and Cho/NAA corresponds with the region of low apparent diffusion coefficient (ADC) values. In panel D, the SVS recorded from the region found to be suspicious for high grade tumor identified (left spectrum TE 30 ms and right long TE 135 ms). The spectroscopy examination reported a region of high grade tumor within a low grade glioma. Positron emission tomography (PET) imaging depicted this tumor as a homogeneous, low-grade tumor, failing to detect the focus of high grade tumor (anaplastic astrocytoma) depicted on MRS and ADC map, which was confirmed on subsequent stereotactic biopsy.

In Figure 20 the SVS is shown, 1.5 T, from a 47 year old woman who had undergone surgery and therapy for glioblastoma multiform. The spectrum shows a reduction in NAA with elevation in choline and lactate concentrations consistent with a recurrent neoplasm. The patient subsequently underwent radiation therapy without the need for biopsy.[112]

The MRS data from three patients with newly diagnosed grade IV gliomas are compared in Figure 21 as described by Catalaa et al.[113] The data were acquired using PRESS

**Table 2. Major $^1$H MRS Metabolites with Peak Assignments, Detection at Short and Long Echo Times (TE) and Role (Marker)[a]**

| ppm | spectral assignment | short TE | long TE | marker |
|---|---|---|---|---|
| 0.9−1.3 | macromolecules, amino acids, lipids | X | | necrotic tumors |
| 1.33 | lactate (Lac) | X | X | anaerobic metabolism |
| 1.47 | alanine (Ala) | X | X | abscess |
| 1.9 | acetate (Ace) | X | X | abscess |
| 2.02, 2.6 | *N*-acetyl aspartate (NAA) | X | X | healthy neuron/invasion |
| 2.05/2.5 | glutamate + glutamine (Glx) | X | | intracellular neurotransmitter |
| 2.4 | pyruvate (Pyr), succinate (Succ) | X | X | pyogenic abscess |
| 3.02, 3.9 | total creatine (Cr) | X | X | energy metabolism |
| 3.2 | total choline (Cho) | X | X | cell membrane metabolism |
| 3.36 | scylloinositol (sI) and taurine (Tau) | X | | PNET[b], some gliomas |
| 3.56, 4.06 | myoinositol (mI), glycine (Gly) | X | | glial proliferation |

[a] Reprinted from the *European Journal of Radiology*, Vol 67, Callot et al. $^1$H MR spectroscopy of human brain tumours: a practical approach, pp 268−274, 2008 with permission from Elsevier.[111] [b] Primitive neuroectodermal tumors.

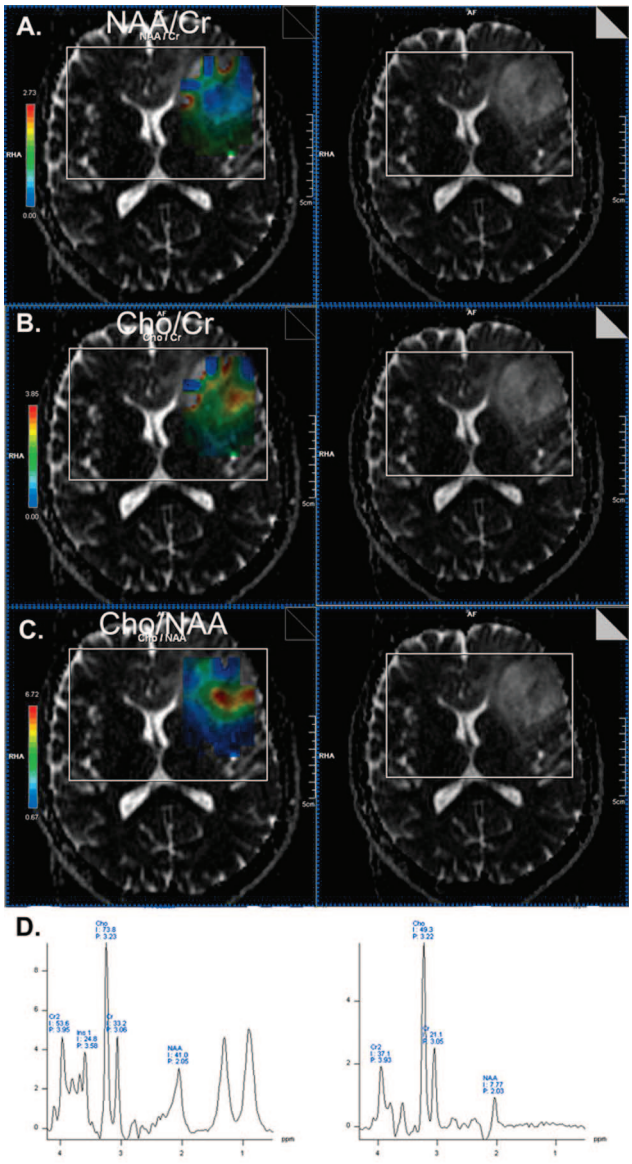


**Figure 19.** Glioma: 3T spectroscopy examination from a low grade glioma containing a focus of high grade tumor (anaplastic astrocytoma) confirmed histologically on stereotactic biopsy. The SI experiment was undertaken with a TE 135 ms, TR 1450 ms, using 16 × 16 phase encoding steps with the region of interest within the PRESS box seen in panels A−C. Left images show the metabolite map reconstructed using the (A) NAA/Cr, (B) Cho/Cr, and (C) Cho/NAA ratio overlaid on an ADC map, which can be viewed on the right. The area of abnormal metabolite signal corresponds with low ADC values. (D) On the left, SVS acquired with TE 30 ms, TR 3000 ms, NAv 96. The spectrum displays greatly reduced NAA signal amplitude, and high Cho/Cr ratio. Additionally strong signals from lipids at 0.9 and 1.3 ppm are seen. On the right, SVS acquired with TE 135 ms, TR 3000 ms, and NAv 96 confirms short-echo findings. Both spectra were recorded from the region of highest Cho and low NAA to record the spectral profile from the region identified on CSI. Data obtained from Stanwell, Cook, Brazier, and Mountford.

and CSI. The spectral grid is superimposed over the top of each of the images. The spectral data is placed below for each patient, and the voxels shaded light gray are suspicious for tumor. The mid-gray voxels are highly suggestive of tumor, and the asterisks indicate the presence of lactate and lipid. Note the large number of voxels with lactate plus lipid, low NAA, and the large variability in choline and creatine levels. The patient in the middle has relatively low choline

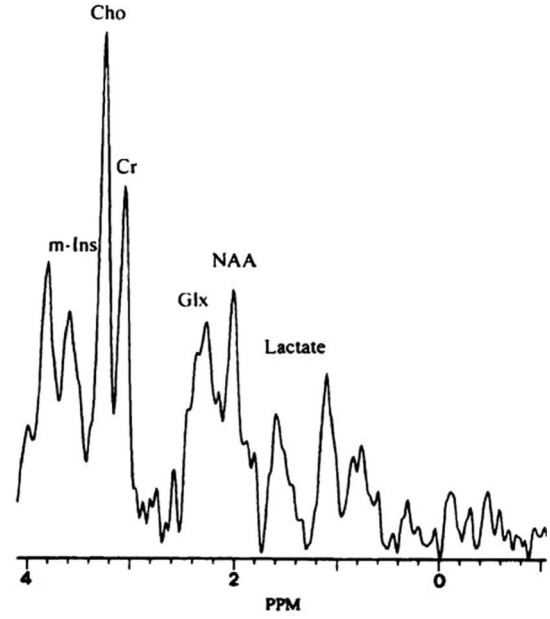


**Figure 20.** Glioblastoma multiforme. SVS PRESS (1500/41) at 1.5 T from a 47 year old woman who had undergone surgery and therapy for glioblastoma multiforme. The resultant spectrum shows a reduction in NAA and elevations in choline and lactate concentrations consistent with a recurrent neoplasm. Cr = creatine and phosphocreatine; Glx = gluatamine/glutamate; m-Ins = myoinositol. Reprinted with permission from Adamson et al, *Radiology*, 1998, vol 209, p 73. Copyright Radiological Society of North America.[112]

levels in the voxels on the edge of the lesion, but the other two patients both have some voxels with very high choline.

**4.3.4.3. Recurrent Tumor.** The spectrum from a healthy control compared with that from a patient with a histologically confirmed recurrent low-grade astrocytoma is seen in Figure 22. The tumor is seen to recur at the posterior margin of prior resection.[110] The spectrum on the right-hand side shows a reduced NAA, increased choline to creatine ratio, and an increase in mI. The level of mI correlates with grade in cerebral astrocytomas.

**4.3.4.4. Survival Analysis.** CSI has been used in conjunction with ADC and relative cerebral blood volume (rCBV) to predict the survival in patients with glioblastoma multiform (GBM). Figure 23 shows a PRESS box superimposed over the MRI. A choline-to-*N*-acetylaspartate index was used to determine that there was a significantly shorter median survival time for patients with a large volume of metabolic abnormality than for those with a small abnormality (12.0 and 17.1 months, respectively, $P = 0.002$). The spectroscopy method was compared with the similar pattern observed for patients with a low ADC value. The authors concluded that the pretreatment volume of the metabolic abnormality in combination with ADC values may be able to predict outcome for patients with GBM.

## *5. Future Challenges*

### 5.1. Hardware and High Field Magnets

For MR spectroscopy, the higher the magnetic field strength the better. As higher field magnets, 7 T and above, become available for human *in vivo* studies, more robust techniques to correct for subject-induced $\mathbf{B}_0$ inhomogeneities need to be developed. Susceptibility differences as a result of tissue−bone or tissue−air interfaces must be corrected if

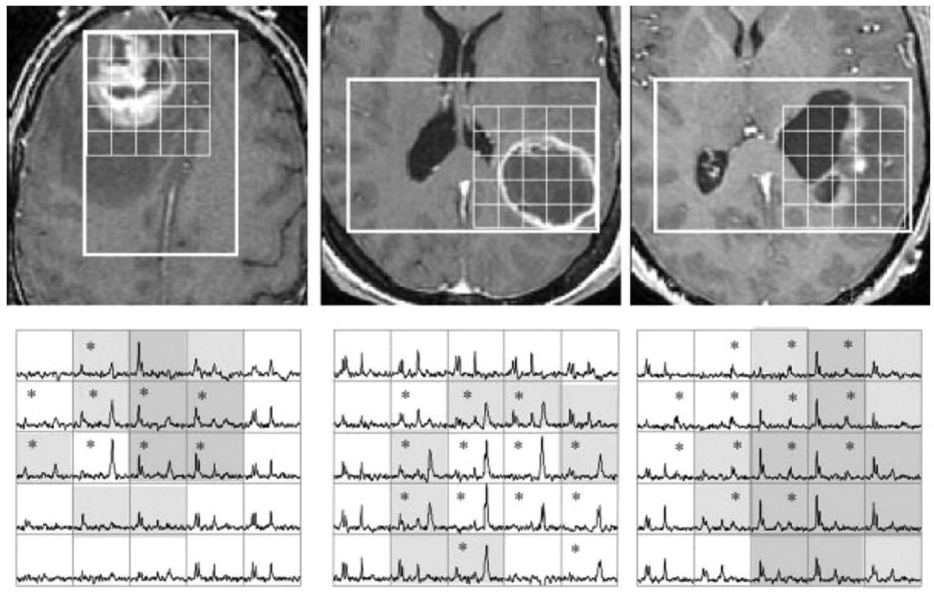

**Figure 21.** Grade IV gliomas. Gadolinium-enhanced $T_1$-weighted MR images and arrays of spectral data from three patients with grade IV gliomas. The MRS data was accrued using the PRESS MRSI method. The voxels shaded light gray are suspicious for tumor, the mid-gray voxels are highly suggestive of tumor and the asterisks indicate lactate and lipid. Note the large number of voxels with lactate plus lipid, low NAA, and the large variability in choline and creatine levels. The patient in the middle has relatively low choline levels in the voxels on the edge of the cyst, but the other two patients both have some voxels with very high choline. Reprinted with permission from Catalaa et al.[113] Copyright 2006 Wiley-Blackwell.

meaningful spectral data is to be acquired. Shimming algorithms[48,114] need to be improved for use at high fields for humans. RF coils[115] are also suggested as a means to reduce $\mathbf{B}_o$ inhomogeneities and thus effort needs to be expended in their redesign.

Higher $\mathbf{B}_o$ fields offer higher SNR but at the same time mean wider spectral widths, shorter $T_2$, and longer $T_1$ relaxation times. Thus, pulse sequences also need to be redesigned. It has been shown in rats that as $\mathbf{B}_o$ increases, spectral resolution improves and $T_1$ and $T_2$ values increase and decrease, respectively; however, SNR levels off above 7 T and may be found to decrease at even higher fields.[116]

A more solid understanding of physical parameters is required to optimize MRS at higher fields with respect to susceptibility variation and magnetic inhomogeneities (varies linearly with $\mathbf{B}_o$), chemical shift artifact (varies linearly with $\mathbf{B}_o$), SNR (varies linearly with $\mathbf{B}o$), specific absorption rate (SAR) (varies linearly with $\mathbf{B}_o^2$), and radiofrequency (inversely proportional to $[\mathbf{B}_o(\varepsilon_r)^{0.5}]$, $\varepsilon_r$ is the relative permittivity), $T_1$ (varies linearly with $\mathbf{B}_o^{1/3}$), and $T_2$ (decreases with increasing $\mathbf{B}_o$).[117,118]

Tkac et al[119,120] acquired human brain SVS at 7 T using a STEAM sequence, 8 mL voxel, and short TE of 6 ms in order to avoid **J**-modulation effects (Figure 24). Outer volume suppressions[121] (OVS) were found necessary to eliminate signal leakage into the voxel, including lipid. In addition to Cho, Cr, NAA resonances, Glu, mI, Tau, and Glucose were identified.

Human brain 7 T CSI feasibility studies have already been carried out[122] and show appreciable improvement in sensitivity and resolution. Proton echo-planar spectroscopic imaging (PEPSI) brain spectra were compared at 1.5, 3, 4, and 7 T[123] in circularly polarized and phase-array coils, where gain in temporal and spectral resolutions, as well as improvement in sensitivity, were observed.

The abundant SNR available at higher $\mathbf{B}_o$ fields, along with higher number of elements per coil, mean that parallel imaging techniques (e.g., sensitivity encoding (SENSE)[124] and generalized autocalibrating partially parallel acquisition (GRAPPA)[125]) are likely to be incorporated into CSI-based methods.[126] With SENSE, reduction of echo train lengths in multiecho sequences can be achieved, which will in turn improve CSI quality.[127] The number of phase-encoding steps can be reduced in SENSE as the number of elements per coil increases, and this will in turn reduce experimental time. GRAPPA application in neuro-CSI (2D proton echo planar spectroscopic imaging "PEPSI") was also able to achieve 5-fold acceleration and shorten experimental time.[126] SENSE combined with turbo-spin−echo-based CSI was also able to achieve an acceleration factor of 9 in the brain.[61]

Shorter RF wavelength (or higher frequency) used at high $\mathbf{B}_o$ fields leads to variable $\mathbf{B}_1$ maps and to flip angle variations across a particular slice. The "central brightening" artifact in water-based phantoms but not in oil based phantoms is a clear manifestation of this problem. This is usually related to the dielectric constant and the conductivity of the medium. Usually, using a multichannel phased-array receive coil eliminates or reduces this type of artifact due to the higher sensitivity of this coil to the outer surface of the tissue. Shimming and/or using multiple transmit SENSE coils[128] can also reduce variation in flip angle across the slice.

SAR is a measure of the rate at which RF energy is absorbed by the body when exposed to radio frequency electromagnetic field. Regulatory SAR limits are fixed, and a major problem is met as RF frequency increases with $\mathbf{B}_o$. Limitation of maximum RF peak powers to stay within acceptable SAR limits means traditional refocusing pulses cannot be employed at high $\mathbf{B}_o$ fields. The wide refocusing bandwidth needed at high $\mathbf{B}_o$ puts higher demand on RF peak powers. Poor $\mathbf{B}_1$ profile selection and flip angle variation of traditional RF pulses lead to the implementation of adiabatic refocusing pulses in CSI sequences with successful application in the brain.[129−131] Due to the wide refocusing bandwidth obtained with an adiabatic refocusing pulse, chemical shift artifacts can be also reduced.

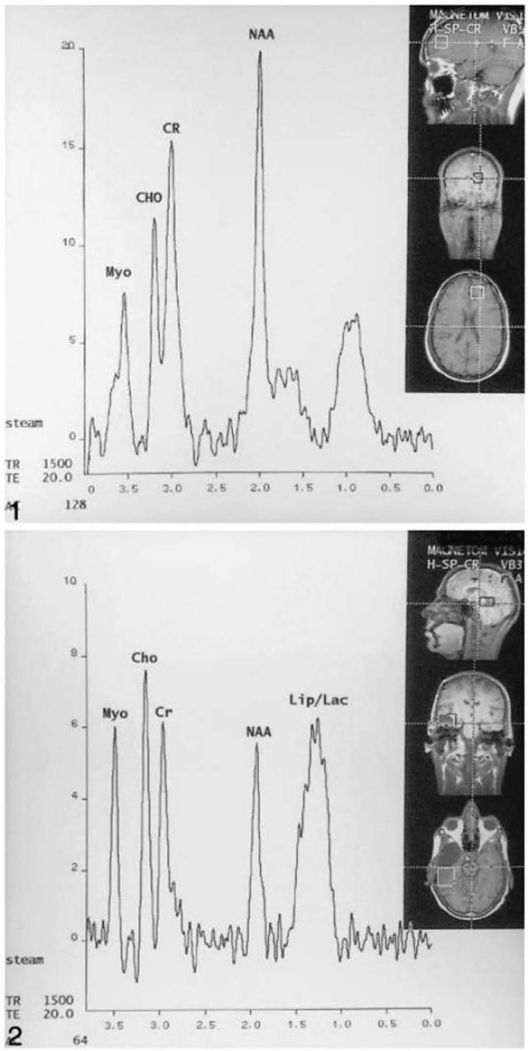


**Figure 22.** Recurrent tumor. Left is the MR spectrum recorded at 1.5 T (TE 20 ms, 2 × 2 × 2 $cm^3$ voxel) from a healthy control subject with the following metabolites: mI (Myo on image), Cho, Cr, and NAA. The small peak at 1.3−1.5 is probably due to lipid contamination (from subcutaneous tissues), which is expected when using this technique. Right is the MR spectrum (TE 20 ms, 3 × 3 × 3 $cm^3$ voxel) obtained from a patient with histologically confirmed, recurrent, low-grade astrocytoma at the posterior margin of prior resection. This shows a high level of mI, mild elevation of Cho, mild decreased NAA, and elevation of lipids and lactate (Lip/Lac) as a sequel of therapy. Reprinted with permission from Castillo, Smith, and Kwock, Correlation of myo-inositol levels and grading of cerebral astrocytomas, *American Journal of Neuroradiology*, Vol. 21 (9), p 1647, 2000. Copyright by American Society of Neuroradiology.[110]

Chemical shift dispersion increases linearly with $\mathbf{B}_o$ and so does chemical shift artifact (CSA), which is a measure of 3D spatial localization error for different chemical shifts that are present within a voxel. This artifact is small at lower fields but can be unacceptable at higher fields without being addressed properly. CSA is proportional to excitation and refocusing bandwidths, which usually decrease at higher $\mathbf{B}_o$ to stay within SAR limits. CSA is more obvious on CSI than on single-voxel exams, and it might lead to signal cancellation and to erroneous results. An adopted solution for this problem at high fields is to use adiabatic refocusing pulses.[132] An adiabatic version of the one-dimension PRESS sequence was proposed by Garwood et al.[132] This is expected to reduce chemical shift artifact and improve quantitation and analysis in 1D neurospectroscopy.

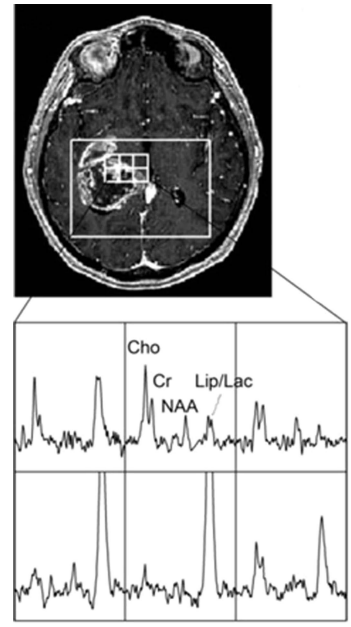


**Figure 23.** Survival analysis. Three-dimensional chemical shift imaging (CSI) (TR/TE =1000/144 ms, phase-encoding matrix = 12 × 12 × 8 or 16 × 8 × 8) with 1 $cm^3$ nominal resolution was acquired with point-resolved spectroscopic (PRESS) volume localization and very selective saturation (VSS) bands use for outer-voxel suppression. The PRESS box was positioned to cover both the lesion and the normal-appearing tissue within 200−300 $cm^3$. Areas of subcutaneous lipid and varying magnetic susceptibility that might compromise the quality of the spectra were avoided. Reprinted from Oh, J.; Henry, R. G.; Pirzkall, A.; Lu, Y.; Li, X.; Catalaa, I.; Chang, S.; Dillon, W. P.; Nelson, S. J. "Survival analysis in patients with glioblastoma multiforme: predictive value of choline-to-N-acetylaspartate index, apparent diffusion coefficient, and relative cerebral blood volume." *J. Magn. Reson. Imaging* 2004 with permission from John Wiley & Sons, Inc.[158]

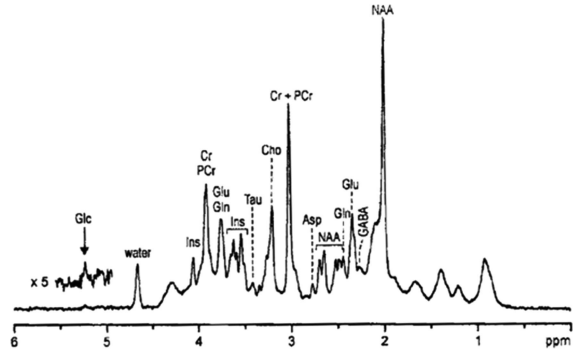


**Figure 24.** Neurospectroscopy at 7 T. *In vivo* $^1$H single voxel MRS of a human brain gray matter at 7 T. Experimental parameters are as follows: pulse sequence, STEAM, with outer volume suppression; TE 6 ms; mixing time 32 ms; TR 5 s; voxel 8 mL; averages 160. Individual FFT and phasing was done before averaging of all scans. Reprinted from Tkac, I.; Andersen, P.; Adriany, G.; Merkle, H.; Ugurbil, K.; Gruetter, R. "In Vivo $^1$H NMR Spectroscopy of the Human Brain at 7 T." *Magnetic Resonance in Medicine* 2001 with permission from John Wiley & Sons, Inc.[119]

STEAM[23] and LASER[132] can both be applied successfully at high fields due to the absence of refocusing pulses in STEAM or three-dimensional selection of voxel by adiabatic pulses in LASER. The sensitivity of acquired signal in a STEAM sequence to $\mathbf{B}_1$ inhomogeneity, which is high at high $\mathbf{B}_o$ fields, is lower than that of PRESS sequences or sequences with 180° RF pulses. The latter reason is one of the reasons why PRESS is not popular at high fields.

Briefly, with more signal available at high $\mathbf{B}_o$, highly resolved and more sensitive spectra can be acquired. The higher SNR also means that parallel imaging techniques can be used to shorten experimental times in CSI studies. Two-dimensional neuro-L-COSY[43,44] and JPRESS[133−135] are also expected to find increased use as better shimming algorithms become available and more adiabatic RF pulses are implemented in spectroscopic sequences.

## 6. New Insight into Biological Mechanisms

### 6.1. Traumatic Brain Injury

Shaken baby syndrome (SBS) is a form of traumatic brain injury (TBI).[40] However the potential fatality of the injury appears to be disproportionate to the mechanical injury sustained. Neurospectroscopy identified a series of biochemical changes that may further the understanding of the mechanisms involved and point to future preventive or therapeutic measures.

The clue lies in the temporal relationship of the metabolite changes that occur with the appearance of lipids early in the time course with the concomitant progressive loss of the neuronal marker, NAA. The loss of NAA coincided with poor neurological outcome, which may indicate that the trauma initiates a lethal neurochemical cascade referred to by Haseler et al.[40] Data accrued at 1.5 T show the three broad resonances (Figure 25) at 0.9, 1.2, and 1.4 ppm consistent with lipid which may have arisen by phospholipase A2 activation, a known cause of neuronal injury.[136−138] An alternative interpretation of the MRS findings is one based upon the presence of unique resonances, first identified in normal neonatal and adult rats and then in adult human brain spectra by Behar[41] as "macromolecules". Seven distinct macromolecules are reported to underlie the normally featureless baseline of the routine brain MRS.

Clues to the origin of the lipid in shaken baby syndrome and traumatic brain injury have come from attempts to mimic the proton spectrum *in vitro* using readily available frozen rat brains and human autopsies. Despite physical disruption, sonication, freeze−thawing, and all variants of mechanical injury, *in vitro* proton MRS failed to identify the resonances of interest. Only after incubation of the pellets at appropriate pH with one of the enzymes phospholipase A2, B, or D did any or all of the "macromolecules" appear in the *in vitro* spectra of the brain. The relationship between mechanical injury *in vivo* and phospholipase A2 release remain speculative, but the striking similarity between *in vivo* and *in vitro* MR spectra suggests a causal link.[91]

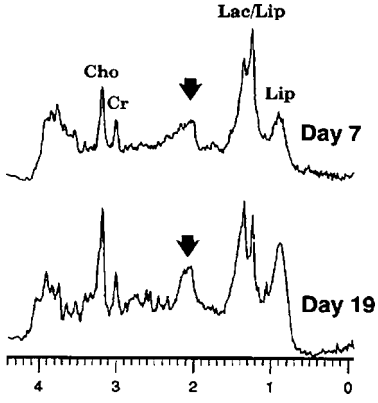


**Figure 25.** Shaken baby syndrome. Proton MR spectra (STEAM, TE = 30 ms, TR = 1500 ms) from an infant at 7 and 19 days post-trauma are grossly abnormal and show almost absent NAA, decreased Cr and mI, and the presence of lactate and lipid peaks. More deterioration is observed at day 19 with increases in lipid. Reproduced with permission from *Pediatrics*, Vol. 99, pp 4−14. Copyright by the AAP.[40]

### 6.2. An Earlier Diagnosis of Alzheimer's Disease

Alzheimer's disease affects millions of Americans each year. It is predicted that one in every three elderly people over the age of 75 will have Alzheimer's disease. The current diagnostic tests for Alzheimer's disease rely on a battery of neurological evaluations based on Diagnostic and Statistical Manual of Mental Disorders criteria. These tests, as with most psychological tests, are often negatively biased by factors such as the patient's education level and language comprehension. Otherwise, the gold standard for diagnosis of Alzheimer's disease is autopsy. This is not conducive for early diagnosis or treatment monitoring.

It has been demonstrated by several studies that neurospectroscopy can distinguish between Alzheimer's disease and other dementias. However, importantly, it may provide an early diagnosis of the disease allowing treatment to begin before the deleterious effects of the disease are irreversible (Figure 26). NAA, the measure of neuronal activity, plays an important role in diagnosis of Alzheimer's disease. As the disease destroys the patient's brain, a loss of neurons occurs, marked by a reduction in NAA.[139] In addition, mI is increased in the brains of Alzheimer's patients.[140] Myoinositol is involved in the phosphoinositol biochemical pathway, which has been found to be disrupted by $\beta$-amyloid plaques found in Alzheimer's disease. Studies comparing postmortem autopsy results and neurospectroscopy during patient lifetime have shown that NAA and mI measurements are 100% sensitive and 75% specific[141] for this diagnosis. Another larger study has shown high correlations between MRS biomarkers of Alzheimer's disease (decreased NAA and increased mI) and postmortem results as well.[142] The MRS AD diagnosis is steadily gaining popularity as physicians realize that it is an accurate and objective test for early detection and treatment monitoring.

Although the neurospectroscopy method shows great promise, the spectral changes that occur in Alzheimer's disease are subtle. Therefore special care must be taken to follow acquisition protocols and postprocessing protocols in order to provide the optimal diagnostic value. For example, it is intuitive that moving from 1.5 to 3.0 T would likely improve the sensitivity of MRS measurements due to the increase in SNR. However in the case of Alzheimer's disease, this is not the case.[143] This is because myoinositol is a pseudosinglet at 1.5 T, whereas due to *J*-coupling effects at 3.0 T, it becomes a multiplet, making it more difficult to measure accurately using standard postprocessing methods. Another subtle but important point is voxel placement. From a pathological point of view, the hippocampus or anteromedial temporal lobe is affected first and most severely by Alzheimer's disease.[144] Spectroscopy in the temporal lobes is technically challenging due to susceptibility differences in the air−tissue interfaces proximal to the temporal lobes. As a result reproducibility of spectra from that region is poor.[145] The posterior cingulate gyrus however is a spectroscopically homogeneous region and therefore is the most diagnostic voxel region for the diagnosis of Alzheimer's disease.[140]

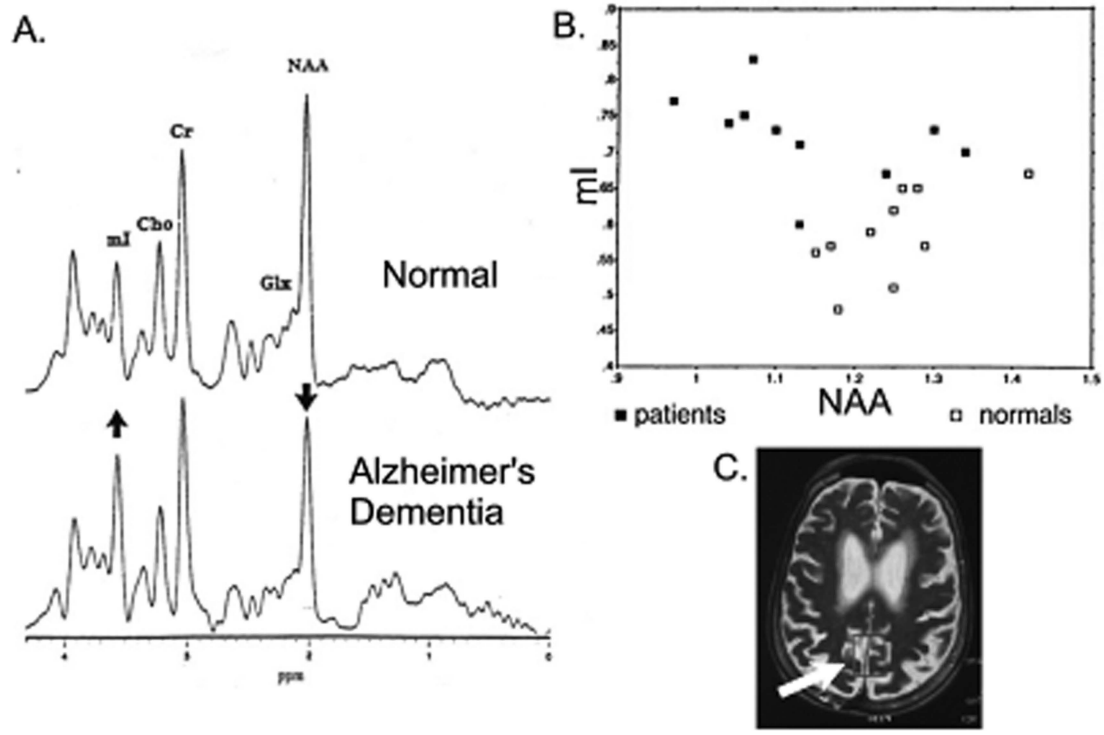


**Figure 26.** Alzheimer's disease. (A) STEAM MRS spectra of normal brain (top) and Alzheimer's diseased brain (bottom). Note the decrease in NAA and increase in mI. (B) Scatter gram of AD patients (■) compared with normative data (□). A differential of NAA and mI clearly separate the two groups. (C) MRS of AD brain with region of interest indicated by the box and arrow. Reprinted from *NeuroRX*, Vol. 2, Lin et al., Efficacy of proton magnetic resonance spectroscopy in neurological diagnosis and neurotherapeutic decision making, pp 197−214, 2005 with permission from Elsevier.[46]

## 6.3. Pain

There has been no objective way of detecting or monitoring pain in a human being.[146] Similarly there was no objective way to prove that a drug was effective other than the patients saying so, and this differs from one person to another. Babies, cognitively impaired adolescents and adults, and the elderly with dementia have had no way to communicate their pain, and the physician had no way to measure it. Those with cognitive function are required to fill in an extensive questionnaire. Since there is no objective test for pain there is also no means of verifying the effectiveness of pain drugs. Many potentially effective drugs are thus not made available.

Acute pain is self-limiting and acts as a warning sign of ongoing tissue damage. It presents as a sensory and emotional response caused by the injury and can last from a few seconds to weeks, but usually goes away with healing. In contrast, chronic pain lasts beyond the typical healing time and is a major health issue. Acute pain serves a protective biological function by acting as a warning of ongoing tissue damage. Chronic pain does not appear to serve a protective biological function; instead it appears to be the symptom of a process that is itself a disease. Chronic pain is unrelenting and not self-limiting and can persist for years and even decades after the initial injury.

There is a need to identify predictive biomarkers of pain and predict the trajectory of pain, as well as the changes in pain over time, for example, acute to chronic. Chronic pain and drug addiction are thought to rely to some degree on shared neurobiological substrates and mechanisms. It is envisioned that a better understanding of these shared central nervous system (CNS) mechanisms will lead to the development of improved analgesics without abuse potential and improved treatments for addiction.

### *6.3.1. Neurospectroscopy and Pain*

Chronic pain causes aberrations to biochemical mechanisms in the brain, and neurospectroscopy is able to monitor changes to chemistry associated with both acute[147,148] and chronic pain.[149−151] Kupers and colleagues have reported an increase in GABA in the frontal cortex associated with acute pain, while others have reported an increase in glutamate (9%) in the anterior cingulate gyrus following the application of a painful stimulus.[147]

However the changes recorded at 1.5 T are small, as seen in Figure 27.[151] At the higher field strength of 3 T (Figure 28), the changes in the choline to creatine ratio are apparent, as are changes in Glx, lipids, amino acids, and mI (Unpublished data, Stanwell, Cousins, Siddall, and Mountford).

### *6.3.2. Pattern Recognition for a Robust Diagnosis of Chronic Pain*

The data reported in Siddall et al[152] were analyzed in two ways: by comparison of individual resonances and assignment of resonances from the literature[24] and by the statistical classification strategy (SCS) method (section 3.19.2), an expert pattern recognition method specifically developed for biomedical spectroscopy data.[71,153] Typical spectra from each brain region (prefrontal cortex, anterior cingulate cortex, and thalamus) of a subject with low back pain are shown in Figure 27.

Thirty-three age-matched healthy and pain-free volunteers were compared with 32 patients with chronic low back pain; the SCS-based pattern recognition method was applied to the MR spectra. The SCS method was able to discriminate low back-pain subjects from control subjects with an accuracy of 100% from the anterior cingulate cortex spectra, 98.5% from

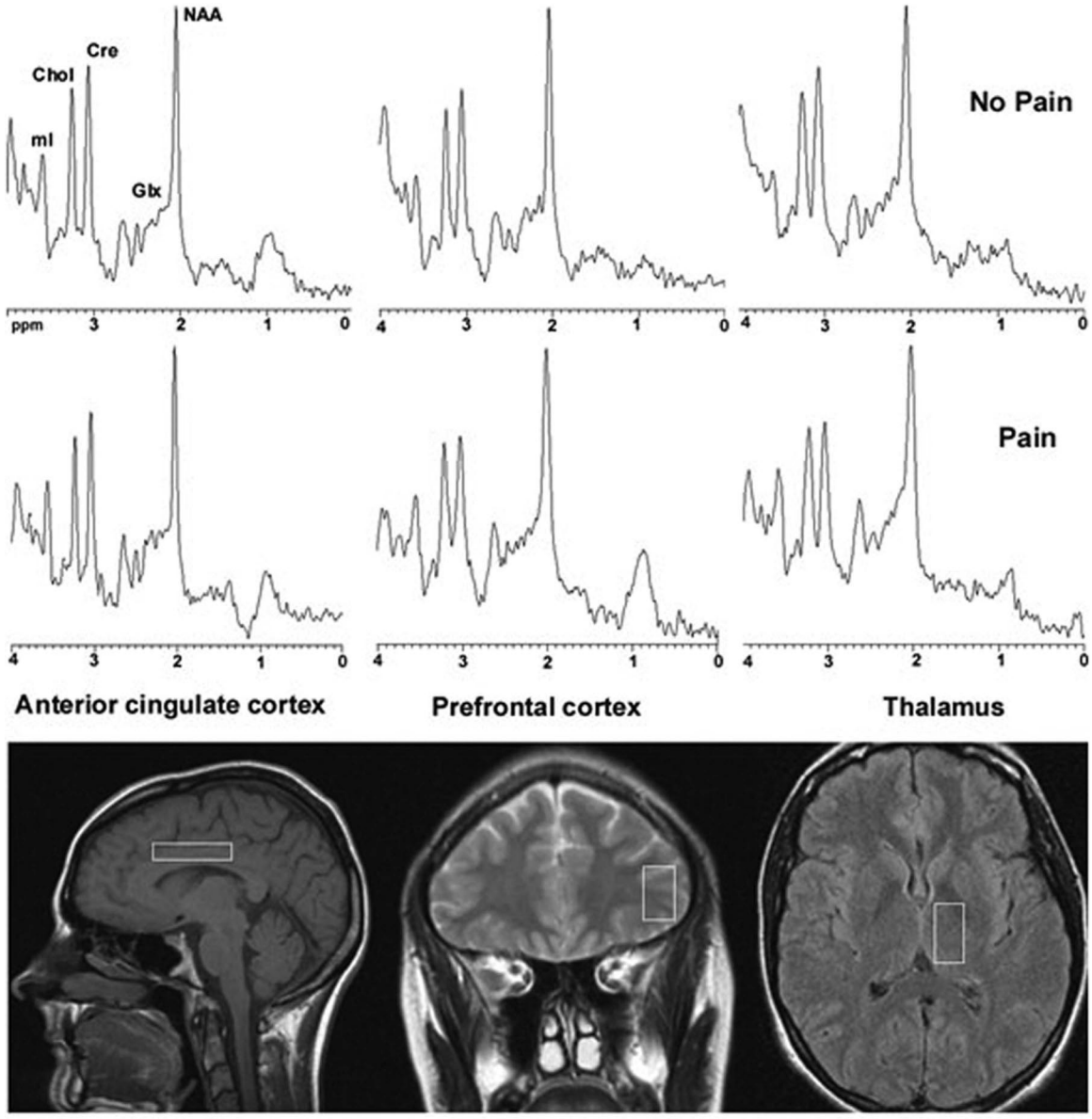


**Figure 27.** Chronic lower back pain at 1.5 T. STEAM typical single-voxel magnetic resonance (MR) spectra collected at 1.5 T from the anterior cingulate cortex, prefrontal cortex, and thalamus using stimulated-echo acquisition mode prescription (TE, 25 ms; TR, 1500 ms; 256 acquistions): top row, healthy volunteer; middle row, low back pain subject; bottom row, box indicates the placement of each single-voxel measurement on the MR image. Chol = choline; Cre = creatine; Glx = glutamine/glutamate; mI = myoinositol; NAA = *N*-acetyl aspartate. Modified from Siddall and Cousins[152] with permission from the International Anesthesia Research Society 2004.

the thalamus spectra, and 96.6% from the prefrontal cortex spectra. The spectral regions identified by the optimum region selection algorithm as optimal for discrimination between the pain and no pain groups are described.[152] Because the searches were nonexhaustive and the sample sizes small (30 plus in each category), there may be other spectral regions not identified that are comparable in discriminatory power.

## 6.4. How Small an Area of Focal Disease Can We See?

At 1.5 T if the disease fills over 30% of the 1 $cm^3$ voxel, then the method will yield a diagnostic result. The higher the magnetic field strength the better the signal-to-noise, but it has yet to be statistically determined how small a lesion can be diagnosed at 3 or 7 T. Currently at our institution, focal lesions of 0.5 $cm^3$ are being recorded (Stanwell, Lin, Mountford, and Ramadan, unpublished data).

## 6.5. How Early Can We Diagnose the Deteriorating Brain?

Mild cognitive impairment in Alzheimer's disease has shown that biochemical changes occur in the brain that precede imaging and symptomatic changes but are also predictive of conversion to the disease.[142,143]

## 6.6. Personalized Medicine or "P4"

Personalized medicine is considered the way of the future. It is also known as "P4" where the four "Ps" are predictive, personalized, preventive, and participatory. The goal is to use each person as their own internal standard and predict and manage disease before it becomes life threatening. Chemistry is a major part of the P4 initiative, and neuro-spectroscopy is one of the early successes. MR does help in the process of imaging and visualizing disease, but by using

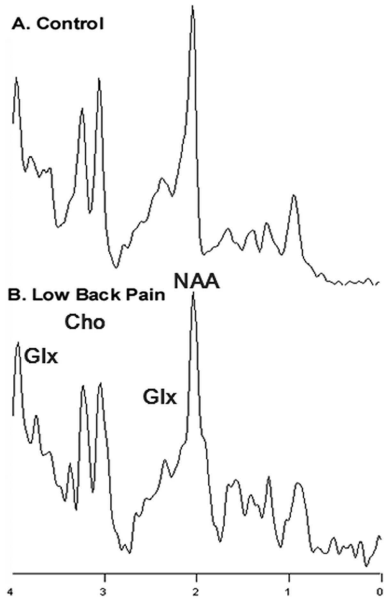


**Figure 28.** Chronic lower back pain at 3 T. Typical single-voxel MR spectra collected at 3 T using STEAM, TE 20 ms, TR 2000 ms: (A) control with no pain; (B) patient with low back pain. Data obtained from Stanwell, Cousins, Siddall, and Mountford.

MRS, we are able to document the precise cause by both epigenetic and genetic changes. MRI and MRS combined with pattern recognition and information technology are already in a position to carry out personalized medicine. The unknown is the "participatory" component, that is, will the governments or individuals pay the price. An excellent example of MRS as P4 medicine is in hypoxic brain injury as described above. Many of the results described in this review illustrate that proton MRS has the necessary attributes for personalize medicine.

## 7. Conclusions

Neurospectroscopy offers a window into the chemistry of the human brain, reporting on normal mechanisms as well as the changes that occur with degeneration, disease, pain, cancer, and infection. The method is also improving our understanding of how each person responds to treatment. Neurospectroscopy is a valuable addition to the current diagnostic methods and is unique in the information it provides.

The long-term effect of shaken baby syndrome and traumatic brain injury can be gauged by neurospectroscopy. For the first time, there is an objective method for the prognosis and hence management of the condition.

Alzheimer's disease can now be identified much earlier than before offering earlier management before the disease progresses.

Neurospectroscopy offers a window to objectively diagnose and understand pain an area that had remained until recently the "Holy Grail" for pain management. Armed with this information, drugs can now be developed and tested and the effects monitored. Infants, the elderly, and the cognitively impaired can now be helped.

In order for the method to become robust for routine diagnosis of all disease types, significant databases need to be collected to allow pattern recognition methods to be implemented as has been achieved for the INTERPRET project[92] and the chronic pain project.[151]

To date the extent of the information available from neurospectroscopy is dependent on the capability of the MR system, operator, and the reader. Neurospectroscopic data is technically a challenge to accrue. Furthermore the interpretation of the data is not so easy when only a small fraction of the ROI contains disease.

The spectral changes that occur in some diseases are subtle, and once these are documented, it is possible to develop spectral filtering methods to extract the precise diagnostic information required. The higher field strength magnets will allow for glutamine and glutamate and GABA to be inspected separately thus allowing the biochemists an insight as to which mechanisms reflect which disease.

With molecular genetics now promising to predict the onset of diseases, a method such as neurospectroscopy is ready to add to the diagnostic armamentaria and find the disease at a time when it can be managed and prior to deterioration of the patient.

## 8. Abbreviations

| | |
|---|---|
| $^{13}C$ | carbon 13 |
| 1D | one dimensional |
| $^{1}H$ | proton |
| 2D | two dimensional |
| AA | Hα of amino acid residues |
| Acyl | acetyl residues |
| ADC | apparent diffusion coefficient |
| AMARES | advanced method for accurate, robust and efficient spectral fitting |
| ATP | adenosine triphosphate |
| BW | bandwidth |
| CHESS | chemical shift selective saturation |
| CHOH | carbohydrate residues (mainly glucose residues from glycogen and free glucose) |
| Cho | choline |
| Chols | choline-containing metabolites |
| Cr | creatine |
| CNS | central nervous system |
| COSY | correlation spectroscopy |
| CPT | current procedural terminology |
| CSA | chemical shift artifact |
| CSI | chemical shift imaging |
| DSS | decision support system |
| FDA | Food and Drug Administration |
| FID | free induction decay |
| FFT | fast Fourier transform |
| GABA | γ-aminobutyric acid |
| GBM | glioblastoma multiform |
| Glc | α- and β-glucose residues |
| GPC | glycerolphosphocholine |
| GRAPPA | generalized autocalibrating partially parallel acquisition |
| H&E | haematoxylin and eosin |
| 1MR | proton magnetic resonance |
| HSQC | heteronuclear single quantum coherence |
| Hz | hertz |
| Inos | inositol |
| Lac | lactate |
| LASER | localization using adiabatic selective refocusing |
| LDA | linear discriminant analysis |
| LGA | linear regression analysis |
| Lip | lipid |
| MR | magnetic resonance |
| MRI | magnetic resonance imaging |
| MRS | magnetic resonance spectroscopy |
| MRUI | magnetic resonance user interface |
| NAA | *N*-acetylaspartate |
| NAAG | *N*-acetylaspartylglutamate |

| | |
|---|---|
| NAv | number of averages |
| NMR | nuclear magnetic resonance |
| NRC | National Research Council, Canada |
| OVS | outer volume suppression |
| PC | phosphocholine |
| PEPSI | proton echo planar spectroscopic imaging |
| ppm | parts per million |
| PRESS | point-resolved spatially localized spectroscopy |
| PRS | pattern recognition systems |
| PROBE | proton brain examination |
| QUEST | quantitation based on quantum estimation |
| RF | radiofrequency |
| ROI | region of interest |
| SAR | specific absorption rate |
| SBS | shaken baby syndrome |
| SCS | statistical classification strategy |
| SENSE | sensitivity encoding |
| SNR | signal-to-noise ratio |
| STEAM | stimulated echo acquisition mode |
| SVS | single-voxel spectrum |
| Tau | taurine |
| TBI | traumatic brain injury |
| UCSF | University of California San Francisco |

## 9. Acknowledgments

The authors would like to thank their co-workers over the years, without whom a multidisciplinary approach such as is described herein would not have been possible. We thank Professors Michael Cousins and Tania Sorrell and Drs. Uwe Himmelreich, Phillip Siddall, and Lavia Gomes for providing unpublished data. We also thank Valerie Graves and Alba Cid for their help in the preparation of this manuscript. We acknowledge the following financial support: ARC DP0663987, NHMRC 153805, Rudi Schulte Research Institute, Santa Barbara, California.

## 10. References

(1) Loudon, G. M. *Organic Chemistry*, 3rd ed.; Benjamin/Cummings Pub. Co.: Redwood City, CA, 1995.
(2) Andrew, E. R. *Philos. Trans. R. Soc., B* **1980**, *289*, 471.
(3) Ernst, R. R. *Biosci. Rep.* **1992**, *12*, 143.
(4) Lauterbur, P. C. *Nature* **1973**, *242*, 190.
(5) de Beer, R.; van den Boogaart, A.; van Ormondt, D.; Pijnappel, W. W.; den Hollander, J. A.; Marien, A. J.; Luyten, P. R. *NMR Biomed.* **1992**, 5.
(6) Luyten, P. R.; Denhollander, J. A. *Radiology* **1986**, *161*, 795.
(7) Vandersprenkel, J. W. B.; Luyten, P. R.; Vanrijen, P. C.; Tulleken, C. A. F.; Denhollander, J. A. *Stroke* **1988**, *19*, 1556.
(8) Chamuleau, R.; Bosman, D. K.; Bovee, W.; Luyten, P. R.; Denhollander, J. A. *NMR Biomed.* **1991**, *4*, 103.
(9) Luyten, P. R.; Marien, A. J. H.; Denhollander, J. A. *NMR Biomed.* **1991**, *4*, 64.
(10) Herholz, K.; Heindel, W.; Luyten, P. R.; Denhollander, J. A.; Pietrzyk, U.; Voges, J.; Kugel, H.; Friedmann, G.; Heiss, W. D. *Ann. Neurol.* **1992**, *31*, 319.
(11) Degraaf, A. A.; Luyten, P. R.; Denhollander, J. A.; Heindel, W.; Bovee, W. *Magn. Reson. Med.* **1993**, *30*, 231.
(12) Frahm, J.; Michaelis, T.; Merboldt, K. D.; Bruhn, H.; Gyngell, M. L.; Hanicke, W. *J. Magn. Reson.* **1990**, *90*, 464.
(13) Frahm, J.; Michaelis, T.; Merboldt, K.; Bruhn, H.; Gyngell, M.; Hanicke, W. *J. Magn. Reson.* **1990**, *90*, 464.
(14) Frahm, J.; Bruhn, H.; Gyngell, M. L.; Merboldt, K. D.; Hanicke, W.; Sauter, R. *Magn. Reson. Med.* **1989**, *11*, 47.
(15) Frahm, J.; Bruhn, H.; Gyngell, M. L.; Merboldt, K. D.; Hanicke, W.; Sauter, R. *Magn. Reson. Med.* **1989**, *9*, 79.
(16) Frahm, J.; Bruhn, H.; Gyngell, M. L.; Merboldt, K. D.; Hanicke, W.; Sauter, R. *Magn. Reson. Med.* **1989**, *9*, 79.
(17) Frahm, J.; Merboldt, K.; Hanicke, W. *J. Magn. Reson.* **1987**, *72*, 502.
(18) Moats, R. A.; Watson, L.; Shonk, T.; Tokuyama, S.; Braslau, D.; Eto, R.; Mandigo, J. C.; Ross, B. D. *J. Comput. Assist. Tomogr.* **1995**, *19*, 480.
(19) Lin, A.; Brooks, M.; Ross, B. D. *Proc. Int. Soc. Magn. Reson. Med.* **2001**, *9*, 2293.
(20) Mountford, C.; Lean, C.; Malycha, P.; Russell, P. *J. Magn. Reson. Imaging* **2006**, *24*, 459.
(21) Mountford, C.; Doran, S.; Lean, C.; Russell, P. *Chem. Rev.* **2004**, *104*, 3677.
(22) Govindaraju, V.; Young, K.; Maudsley, A. A. *NMR Biomed.* **2000**, 129.
(23) Frahm, J.; Merboldt, K.; Hanicke, W. *J. Magn. Reson.* **1987**, *72*, 502.
(24) Danielsen, E.; Ross, B. *Magnetic Resonance Spectroscopy: Diagnosis of Neurological Diseases*; Marcel Dekker: New York, 1999.
(25) Kreis, R.; Farrow, N. A.; Ross, B. D. *Lancet* **1990**, *336*, 635.
(26) Kreis, R.; Ernst, T.; Ross, B. D. *J. Magn. Reson.* **1993**, *102*, 9.
(27) Kreis, R.; Ernst, T.; Ross, B. D. *Magn. Reson. Med.* **1993**, *30*, 1.
(28) Moffett, J. R.; Namboodiri, M. A.; Neale, J. H. *J. Histochem. Cytochem.* **1993**, *41*, 559.
(29) Ross, B. D. *IUBMB Life* **2000**, *50*, 177.
(30) Cooper, J. R.; Bloom, F. E.; Roth, R. H. *The Biochemical Basis of Neuropharmacology*; Oxford University Press: New York, 1970.
(31) Baslow, M. H. *J. Neurochem.* **2000**, *75*, 453.
(32) Chakraborty, G.; Mekala, P.; Yahya, D.; Wu, G.; Ledeen, R. W. *J. Neurochem.* **2001**, *78*, 736.
(33) Ross, B. D. *NMR Biomed.* **1991**, *4*, 59.
(34) Bluml, S.; Moreno, A.; Hwang, J. H.; Ross, B. D. *NMR Biomed.* **2001**, *14*, 19.
(35) Bluml, S.; Seymour, K. J.; Ross, B. D. *Magn. Reson. Med.* **1999**, *42*, 643.
(36) Ross, B. D.; Bluml, S.; Cowan, R.; Danielsen, E.; Farrow, N.; Gruetter, R. *Biophys. Chem.* **1997**, *68*, 161.
(37) Ross, B. D.; Danielsen, E. R.; Bluml, S. *Dig. Dis.* **1996**, *14* (Suppl 1), 30.
(38) Ross, B. D.; Bluml, S. *NMR Biomed.* **1996**, *9*, 279.
(39) Ross, B. D. *NMR Biomed.* **1992**, *5*, 215.
(40) Haseler, L. J.; Arcinue, E.; Danielsen, E. R.; Bluml, S.; Ross, B. D. *Pediatrics* **1997**, *99*, 4.
(41) Behar, K. L.; Rothman, D. L.; Spencer, D. D.; Petroff, O. A. *Magn. Reson. Med.* **1994**, *32*, 294.
(42) Aue, W. P.; Bartholdi, E.; Ernst, R. R. *J. Chem. Phys.* **1976**, *64*, 2229.
(43) Thomas, M. A.; Yue, K.; Binesh, N.; Davanzo, P.; Kumar, A.; Siegel, B.; Frye, M.; Curran, J.; Lufkin, R.; Martin, P.; Guze, B. *Magn. Reson. Med.* **2001**, *46*, 58.
(44) Ziegler, A.; Gillet, B.; Belloeil, J. C.; Macher, J. P.; Decorps, M.; Nedelec, J. C. *Magn. Reson. Mater. Phys., Biol. Med.* **2001**, *14*, 45.
(45) Lin, A.; Nguy, C. H.; Shic, F.; Ross, B. D. *Toxicol. Lett.* **2001**, *123*, 169.
(46) Lin, A.; Ross, B. D.; Harris, K.; Wong, W. *NeuroRX* **2005**, *2*, 197.
(47) Kreis, R. *Prog. Nucl. Magn. Reson. Spectrosc.* **1997**, *31*, 155.
(48) Gruetter, R. *Magn. Reson. Med.* **1993**, *29*, 804.
(49) Kanayamay, S.; Kuhara, S.; Satoh, K. *Magn. Reson. Med.* **1996**, *36*, 637.
(50) Spielman, D. M.; Adalsteinsson, E.; Lim, K. O. *Magn. Reson. Med.* **1998**, *40*, 376.
(51) Ogg, R. J.; Kingsley, P. B.; Taylor, J. S. *J. Magn. Reson. Ser. B* **1994**, *104*, 1.
(52) Haase, A.; Frahm, J.; Hanicke, W.; Matthaei, D. *Phys. Med. Biol.* **1985**, *30*, 341.
(53) Lin, A. P. In *Modern Magnetic Resonance*; Webb, G., Ed.; Kluwer Academic Publishers: London, 2008; Vol. 3, p 985.
(54) Von Kienlin, M. Presented at the International Society for Magnetic Resonance in Medicine, Twelfth Scientific Meeting, Educational Committee Kyoto, Japan, 2004.
(55) Bottomley, P. A. *Ann. N.Y. Acad. Sci.* **1987**, *508*, 333.
(56) Mao, J.; Mareci, T. H.; Andrew, E. R. *J. Magn. Reson.* **1988**, *79*, 1.
(57) Matson, G. B. *Magn. Reson. Imaging* **1994**, *12*, 1205.
(58) Pauly, J.; Leroux, P.; Nishimura, D.; Macovski, A. *IEEE Trans. Med. Imaging* **1991**, *10*, 53.
(59) Maudsley, A. A.; Hilal, S. K.; Perman, W. H.; Simon, H. E. *J. Magn. Reson.* **1983**, *51*, 147.
(60) Maudsley, A. A.; Matson, G. B.; Hugg, J. W.; Weiner, M. W. *Magn. Reson. Med.* **1994**, *31*, 645.
(61) Dydak, U.; Pruessmann, K. P.; Weiger, M.; Tsao, J.; Meier, D.; Boesiger, P. *Magn. Reson. Med.* **2003**, *50*, 196.
(62) Mierisová, S.; Ala-Korpela, M. *NMR Biomed.* **2001**, *14*, 247.
(63) Vanhamme, L.; Sundin, T.; Van Hecke, P.; Van Huffel, S. *NMR Biomed.* **2001**, *14*, 233.
(64) Slotboom, J.; Boesch, C.; Kreis, R. *Magn. Reson. Med.* **1998**, *39*, 899.
(65) Witjes, H.; Melssen, W. J.; Zandt, H. J. A.; van der Graaf, M.; Heerschap, A.; Buydens, L. M. C. *J. Magn. Reson.* **2000**, *144*, 35.
(66) in 't Zandt, H. J. A.; van der Graaf, M.; Heerschap, A. *NMR Biomed.* **2001**, *14*, 224.
(67) Freeman, R. *A Handbook of Nuclear Magnetic Resonance*; 2nd ed.; Longman Publishing Group: Harlow, U.K., 1997.
(68) de Graaf, A. A.; Bovee, W. M. *Magn. Reson. Med.* **1990**, *15*, 305.

(69) Cavassila, S.; Deval, S.; Huegen, C.; van Ormondt, D.; Graveron-Demilly, D. *J. Magn. Reson.* **2000**, *143*, 311.
(70) Preul, M.; Caramanos, Z.; Collins, D.; Villemure, J.-G.; Leblanc, R.; Olivier, A.; Pokrupa, R.; Arnold, D. *Nat. Med.* **1996**, *2*, 323.
(71) Somorjai, R. L.; Alexander, M.; Baumgartner, R.; Booth, S.; Bowman, C.; Demko, A.; Dolenko, B.; Mandelzweig, M.; Nikulin, A. E.; Pizzi, N.; Pranckeviciene, E.; Summers, R.; Zhilkin, P. In *Artificial Intelligence Methods and Tools for Systems Biology*; Dubitzky, W., Azuaje, F., Eds.; Springer and Kluwer: Boston, MA, 2004.
(72) van den Boogaart, A.; Ala-Korpela, M.; Howe, F. A.; Rodrigues, L. M.; Stubbs, M.; Griffiths, J. R. *Magn. Reson. Mater. Phys., Biol. Med.* **1994**, *2*, 479.
(73) Elster, C.; Link, A.; Schubert, F.; Seifert, F.; Walzel, M.; Rinneberg, H. *Magn. Reson. Imaging* **2000**, *18*, 597.
(74) Poullet, J.-B.; Sima, D. M.; Van Huffel, S. *J. Magn. Reson.* **2008**, *195*, 134.
(75) Naressi, A.; Couturier, C.; Devos, J.; Janssen, M.; Mangeat, C.; Beer, R.; Graveron-Demilly, D. *Magn. Reson. Mater. Phys., Biol. Med.* **2001**, *12*, 141.
(76) http://www.mrui.uab.es/mrui/mruiHomePage.html.
(77) Vanhamme, L.; van den Boogaart, A.; Van Huffel, S. *J. Magn. Reson.* **1997**, *129*, 35.
(78) Ratiney, H.; Sdika, M.; Coenradie, Y.; Cavassila, S.; van Ormondt, D.; Graveron-Demilly, D. *NMR Biomed.* **2005**, *18*, 1.
(79) Provencher, S. W. *Magn. Reson. Med.* **1993**, *30*, 672.
(80) Antoine, J.-P.; Chauvin, C.; Coron, A. *NMR Biomed.* **2001**, *14*, 265.
(81) Antoine, J.-P.; Coron, A.; Derepp, J.-M. *J. Magn. Reson.* **2000**, *144*, 189.
(82) Young, K.; Soher, B. J.; Maudsley, A. A. *Magn. Reson. Med.* **1998**, *40*, 816.
(83) Gillies, P.; Marshall, I.; Asplund, M.; Winkler, P.; Higinbotham, J. *NMR Biomed.* **2006**, *19*, 617.
(84) Serrai, H.; Senhadji, L.; Clayton, D. B.; Zuo, C.; Lenkinski, R. E. *J. Magn. Reson.* **2001**, *149*, 45.
(85) Serrai, H.; Senhadji, L.; de Certaines, J. D.; Coatrieux, J. L. *J. Magn. Reson.* **1997**, *124*, 20.
(86) El-Deredy, W. *NMR Biomed.* **1997**, *10*, 99.
(87) Hagberg, G. *NMR Biomed.* **1998**, *11*, 148.
(88) Lindon, J. C.; Holmes, E.; Nicholson, J. K. *Prog. Nucl. Magn. Reson. Spectrosc.* **2001**, *39*, 1.
(89) Sajda, P. *Annu. Rev. Biomed. Eng.* **2006**, *8*, 537.
(90) Lean, C. L.; Somorjai, R. L.; Smith, I. C. P.; Russell, P.; Mountford, C. E. In *Annual Reports NMR Spectroscopy*; Webb, G., Ed.; Academic Press: Guildford, U.K., 2002; Vol. 48, p 71.
(91) Farooqui, A. A.; Horrocks, L. A. *Neuroscientist* **2006**, *12*, 245.
(92) Tate, A. R.; Underwood, J.; Acosta, D. M.; Julia-Sape, M.; Majos, C.; Moreno-Torres, A.; Howe, F. A.; van der Graaf, M.; Lefournier, V.; Murphy, M. M.; Loosemore, A.; Ladroue, C.; Wesseling, P.; Luc Bosson, J.; Cabanas, M. E.; Simonetti, A. W.; Gajewicz, W.; Calvar, J.; Capdevila, A.; Wilkins, P. R.; Bell, B. A.; Remy, C.; Heerschap, A.; Watson, D.; Griffiths, J. R.; Arus, C. *NMR Biomed.* **2006**, *19*, 411.
(93) Ross, B. D.; Enriquez, C.; Lin, A. P. In *Clinical MR Neuroimaging*; Gillard, J. H., Waldman, A. D., Barker, P. B., Eds.; Cambridge University Press: Cambridge, U.K., 2005, p 690.
(94) Kreis, R.; Arcinue, E.; Ernst, T.; Shonk, T. K.; Flores, R.; Ross, B. D. *J. Clin. Invest.* **1996**, *97*, 1142.
(95) Ross, B. D.; Ernst, T.; Kreis, R.; Haseler, L. J.; Bayer, S.; Danielsen, E.; Bluml, S.; Shonk, T.; Mandigo, J. C.; Caton, W.; Clark, C.; Jensen, S. W.; Lehman, N. L.; Arcinue, E.; Pudenz, R.; Shelden, C. H. *J. Magn. Reson. Imaging* **1998**, *8*, 829.
(96) Ashwal, S.; Holshouser, B. A.; Shu, S. K.; Simmons, P. L.; Perkin, R. M.; Tomasi, L. G.; Knierim, D. S.; Sheridan, C.; Craig, K.; Andrews, G. H.; Hinshaw, D. B. *Pediatr. Neurol.* **2000**, *23*, 114.
(97) Kadri, M.; Shu, S.; Holshouser, B.; Deming, D.; Hopper, A.; Peverini, R.; Ashwal, S. *J. Perinatol.* **2003**, *23*, 181.
(98) Hollingworth, W.; Medina, L. S.; Lenkinski, R. E.; Shibata, D. K.; Bernal, B.; Zurakowski, D.; Comstock, B.; Jarvik, J. G. *AJNR Am. J. Neuroradiol.* **2006**, *27*, 1404.
(99) Lin, A.; Ross, B. D.; Harris, K.; Wong, W. *NeuroRx* **2005**, *2*, 197.
(100) Favre, J.; Taha, J. M.; Burchiel, K. J. *Neurosurgery* **2002**, *50*, 48.
(101) Hall, W. *Cancer* **2000**, *82*, 1749.
(102) Garg, M.; Gupta, R. K.; Husain, M.; Chawla, S.; Chawla, J.; Kumar, R.; Rao, S. B.; Misra, M. K.; Prasad, K. N. *Radiology* **2004**, *230*, 519.
(103) Pandit, L. A.; Gahbauer, H.; Libertin, C. R.; Erdogan, B. *J. Comput. Assist. Tomogr.* **2001**, *25*, 950.
(104) Chang, K. H.; Song, I. C.; Kim, S. H.; Han, M. H.; Kim, H. D.; Seong, S. O.; Jung, H. W.; Han, M. C. *AJNR Am. J. Neuroradiol.* **1998**, *19*, 401.
(105) Chen, T.; Farrow, N.; Bluml, S.; Huang, C.; Ross, B. D. *Proc. Int. Soc. Magn. Reson. Med.* **1998**, *6*, 537.
(106) Lin, A.; Bluml, S.; Mamelak, A. N. *J. Neurooncol.* **1999**, *45*, 69.
(107) Aboagye, E. O.; Bhujwalla, Z. M. *Cancer Res.* **1999**, *59*, 80.
(108) Warberg, O. *Science* **1956**, *123*, 309.
(109) Negendank, W.; Sauter, R. *Anticancer Res.* **1996**, *16*, 1533.
(110) Castillo, M.; Smith, J. K.; Kwock, L. *AJNR Am. J. Neuroradiol.* **2000**, *21*, 1645.
(111) Callot, V.; Galanaud, D.; Le Fur, Y.; Confort-Gouny, S.; Ranjeva, J. P.; Cozzone, P. J. *Eur. J. Radiol.* **2008**, *67*, 268.
(112) Adamson, A. J.; Rand, S. D.; Prost, R. W.; Kim, T. A.; Schultz, C.; Haughton, V. M. *Radiology* **1998**, *209*, 73.
(113) Catalaa, I.; Henry, R.; Dillon, W. P.; Graves, E. E.; McKnight, T. R.; Lu, Y.; Vigneron, D. B.; Nelson, S. J. *NMR Biomed.* **2006**, *19*, 463.
(114) Miyasaka, N.; Takahashi, K.; Hetherington, H. P. *Magn. Reson. Med.* **2006**, *55*, 198.
(115) Avdievich, N. I.; Hetherington, H. P.; Kuznetsov, A. M.; Pan, J. W. *J. Magn. Reson. Imaging* **2009**, *29*, 461.
(116) de Graaf, R. A.; Brown, P. B.; McIntyre, S.; Nixon, T. W.; Behar, K. L.; Rothman, D. L. *Magn. Reson. Med.* **2006**, *56*, 386.
(117) Bernstein, M. A.; Huston, J.; Ward, H. A. *J. Magn. Reson. Imaging* **2006**, *24*, 735.
(118) Dydak, U.; Schar, M. *Neuroimaging Clin. N. Am.* **2006**, *16*, 269.
(119) Tkac, I.; Andersen, P.; Adriany, G.; Merkle, H.; Ugurbil, K.; Gruetter, R. *Magn. Reson. Med.* **2001**, *46*, 451.
(120) Tkac, I.; Gruetter, R. *Appl. Magn. Reson.* **2005**, *29*, 139.
(121) Tran, T. K. C.; Vigneron, D. B.; Sailasuta, N.; Tropp, J.; Le Roux, P.; Kurhanewicz, J.; Nelson, S.; Hurd, R. *Magn. Reson. Med.* **2000**, *43*, 23.
(122) Xu, D.; Cunningham, C. H.; Chen, A. P.; Li, Y.; Kelley, D. A. C.; Mukherjee, P.; Pauly, J. M.; Nelson, S. J.; Vigneron, D. B. *Magn. Reson. Imaging* **2008**, *26*, 1201.
(123) Otazo, R.; Mueller, B.; Ugurbil, K.; Wald, L.; Posse, S. *Magn. Reson. Med.* **2006**, *56*, 1200.
(124) Pruessmann, K. P.; weiger, M.; Scheidegger, M. B.; Boesiger, P. *Magn. Reson. Med.* **1999**, *42*, 952.
(125) Griswold, M. A.; Jakob, P. M.; Heidemann, R. M.; Nittka, M.; Jellus, V.; Wang, J.; Kiefer, B.; Haase, A. *Magn. Reson. Med.* **2002**, *47*, 1202.
(126) Shang-Yueh, Tsai; Otazo, R.; Posse, S.; Lin, Y.-R.; Chung, H.-W.; Wald, L. L.; Wiggins, G. C.; Lin, F.-H. *Magn. Reson. Med* **2008**, *59*, 989.
(127) Dydak, U.; Weiger, M.; Pruessmann, K. P.; Meier, D.; Boesiger, P. *Magn. Reson. Med.* **2001**, *46*, 713.
(128) Ullmann, P.; Junge, S.; Wick, M.; Seifert, F.; Ruhm, W.; Hennig, J. *Magn. Reson. Med.* **2005**, *54*, 994.
(129) Scheenen, T.; Klomp, D.; Wijnen, J.; Heerschap, A. *Proc. Int. Soc. Magn. Reson. Med.* **2007**, 43.
(130) Scheenen, T. W. J.; Heerschap, A.; Klomp, D. W. J. *Magn. Reson. Mater. Phys., Biol. Med.* **2008**, *21*, 95.
(131) Ramadan, S.; Ratai, E. M.; Andronesi, O. C.; Sorensen, A. G.; Mountford, C. E. *Proc. Int. Soc. Magn. Reson. Med.* **2009**, in press.
(132) Garwood, M.; DelaBarre, L. *J. Magn. Reson.* **2001**, 153.
(133) Thomas, M. A.; Hattori, N.; Umeda, M.; Sawada, T.; Naruse, S. *NMR Biomed.* **2003**, *16*, 245.
(134) Kim, H.-W.; Buckley, D. L.; Peterson, D. M.; Duensing, G. R.; Caserta, J.; Fitzsimmons, J.; Blackband, S. J. *Invest. Radiol.* **2003**, *38*, 443.
(135) Ryner, L. N.; Sorenson, J. A.; Thomas, M. A. *Magn. Reson. Imaging* **1995**, *13*, 853.
(136) Muralikrishna Adibhatla, R.; Hatcher, J. F. *Free Radical Biol. Med.* **2006**, *40*, 376.
(137) Phillis, J. W.; O'Regan, M. H. *Crit. Rev. Neurobiol.* **2003**, *15*, 61.
(138) Verity, M. A. *Ann. N.Y. Acad. Sci.* **1993**, *679*, 110.
(139) Moats, R. A.; Ernst, T.; Shonk, T. K.; Ross, B. D. *Magn. Reson. Med.* **1994**, *32*, 110.
(140) Kantarci, K.; Jack, C. R., Jr.; Xu, Y. C.; Campeau, N. G.; O'Brien, P. C.; Smith, G. E.; Ivnik, R. J.; Boeve, B. F.; Kokmen, E.; Tangalos, E. G.; Petersen, R. C. *Neurology* **2000**, *55*, 210.
(141) Lin, A.; Schic, F.; Ross, B. D. *Neurology* **2010**, in press.
(142) Kantarci, K.; Knopman, D. S.; Dickson, D. W.; Parisi, J. E.; Whitwell, J. L.; Weigand, S. D.; Josephs, K. A.; Boeve, B. F.; Petersen, R. C.; Jack, C. R., Jr. *Radiology* **2008**, *248*, 210.
(143) Kantarci, K.; Reynolds, G.; Petersen, R. C.; Boeve, B. F.; Knopman, D. S.; Edland, S. D.; Smith, G. E.; Ivnik, R. J.; Tangalos, E. G.; Jack, C. R., Jr. *AJNR Am. J. Neuroradiol.* **2003**, *24*, 843.
(144) Cummings, J. L. *N. Engl. J. Med* **2004**, *351*, 56.
(145) Soher, B. J.; Vermathen, P.; Schuff, N.; Wiedermann, D.; Meyerhoff, D. J.; Weiner, M. W.; Maudsley, A. A. *Magn. Reson. Imaging* **2000**, *18*, 1159.
(146) Cepeda, M.; Cousins, M.; Carr, D. *Fast Facts: Chronic Pain* Health Press: Oxford, U.K., 2007.
(147) Mullins, P.; Rowland, L.; Junga, R.; Sibbitt, W. *Neuroimage* **2005**, *26*, 642.
(148) Kupers, R.; Danielsen, E.; Kehlet, H.; Christensen, R.; Thomsen, C. *Pain* **2009**, *142*, 89.
(149) Grachev, I. D.; Fredrickson, B. E.; Apkarian, A. V. *Pain* **2000**, *89*, 7.

(150) Pattany, P. M.; Yezierski, R. P.; Widerström-Noga, E. G.; Bowen, B. C.; Martinez-Arizala, A.; Garcia, B. R.; Quencer, R. M. *AJNR Am. J. Neuroradiol.* **2002**, *23*, 901.
(151) Siddall, P. J.; Stanwell, P.; Woodhouse, A.; Somorjai, R. L.; Dolenko, B.; Nikulin, S.; Bourne, R.; Himmelreich, U.; Lean, C. L.; Cousins, M. J.; Mountford, C. E. *Anesth. Analg.* **2006**, *102*, 1164.
(152) Siddall, P. J.; Cousins, M. J. *Anesth. Analg.* **2004**, *99*, 510.
(153) Somorjai, R.; Dolenko, B.; Baumgartner, R. *Bioinformatics* **2003**, *19*, 1484.
(154) Ross, B.; Bluml, S. *Anat. Rec.* **2001**, *265*, 54.
(155) Stanwell, P.; Mountford, C. E. *RadioGraphics* **2007**, *2007*, S253.
(156) Dzendrowskyj, T. Application of magnetic resonance to classify cerebral infection and tumour. PhD Thesis, University of Sydney, Sydney Australia, 2002.
(157) Pandit, S.; Lin, A.; Gahbauer, H.; Libertin, C. R.; Erdogan, B. *J. Comput. Assist. Tomogr.* **2001**, *25*, 950.
(158) Oh, J.; Henry, R. G.; Pirzkall, A.; Lu, Y.; Li, X.; Catalaa, I.; Chang, S.; Dillon, W. P.; Nelson, S. J. *J. Magn. Reson. Imaging* **2004**, *19*, 546.

CR900250Y